Geometry and dynamics of mildly degenerate Hopf–Neĭmarck–Sacker families near resonance

Broer, Hendrik; Holtman, S.J.; Vegter, Geert; Vitolo, R.

Published in:
Nonlinearity

IOP PUBLISHING NONLINEARITY

Nonlinearity **22** (2009) 2161–2200 doi:10.1088/0951-7715/22/9/007

Geometry and dynamics of mildly degenerate Hopf–Neĭmarck–Sacker families near resonance

H W Broer[1], **S J Holtman**[1], **G Vegter**[1] **and R Vitolo**[2]

[1] Institute for Mathematics and Computer Science, University of Groningen, PO Box 407, 9700 AK Groningen, The Netherlands
[2] School of Engineering, Computing and Mathematics, University of Exeter, North Park Road, Exeter EX4 4QF, UK

E-mail: H.W.Broer@math.rug.nl, S.J.Holtman@math.rug.nl, G.Vegter@math.rug.nl and R.Vitolo@exeter.ac.uk

Received 5 December 2008, in final form 27 June 2009
Published 30 July 2009
Online at stacks.iop.org/Non/22/2161

Recommended by Y G Kevrekidis

Abstract

This paper deals with families of planar diffeomorphisms undergoing a Hopf–Neĭmarck–Sacker bifurcation and focuses on bifurcation diagrams of the periodic dynamics. In our universal study the corresponding geometry is classified using Lyapunov–Schmidt reduction and contact-equivalence singularity theory, equivariant under an appropriate cyclic group. This approach recovers the non-degenerate standard Arnol'd resonance tongues. Our main concern is a mildly degenerate case, for which we analyse a 4-parameter universal model in detail. The corresponding resonance set has a Whitney stratification, which we explain by giving its incidence diagram and by giving both two- and three-dimensional cross-sections of parameter space. We investigate the further complexity of the dynamics of the universal model by performing a bifurcation study of an approximating family of Takens normal form vector fields. In particular, this study demonstrates how the bifurcation set extends an approximation of the resonance set of the universal model.

Mathematics Subject Classification: 37G15, 37G40, 34C25

(Some figures in this article are in colour only in the electronic version)

1. Introduction

Setting of the problem. We continue our study [5, 7] of resonance sets and their boundaries for non-degenerate and mildly degenerate Hopf–Neĭmarck–Sacker (HNS) bifurcations of families of planar diffeomorphisms. We recall that a HNS bifurcation occurs if a family has at least one

real parameter, which under an appropriate variation causes the pair of conjugate eigenvalues at a fixed point to cross the unit circle transversally [1, 12, 23]. As a consequence, an invariant circle branches off the fixed point, which also undergoes a change in stability. The dynamics on the invariant circle is either periodic or quasi-periodic. We focus on the periodic case, requiring that the eigenvalues of a specific member of the family, the central singularity, are of the form $e^{\pm 2\pi i p/q}$ with $\gcd(p, q) = 1$. This situation may lead to resonance sets, which are regions in parameter space corresponding to the occurrence of q-periodic orbits near the fixed point of the central singularity, and the boundaries of these sets correspond to the appearance or merging of such periodic orbits, typically through a saddle-node bifurcation [5].

Our aim is to go one step beyond the classical scenario, which corresponds to the non-degenerate case. Excluding strong resonances ($q \leqslant 4$), it is well known that a generic 2-parameter family has a tongue shaped resonance set in this situation [1, 5, 23]. Upon passage of the corresponding boundaries a pair of q-periodic orbits appears or merges. For $q \geqslant 7$ a novel mildly degenerate situation can be encountered, which occurs in generic 4-parameter families. In this case there are bifurcations of up to four q-periodic orbits near the central singularity [5].

In [7] we obtain universal models for non-degenerate and mildly degenerate families of diffeomorphisms using Lyapunov–Schmidt reduction and $\mathbb{Z}_q$-equivariant contact-equivalence singularity theory. These universal models, depending on two and four parameters, respectively, determine the local geometry of the resonance sets in generic families.

Our contribution is twofold. The main issue is the description of the resonance set of the mildly degenerate 4-parameter model of [5], which has a Whitney stratification. We present the corresponding incidence diagram and both two-dimensional and three-dimensional tomograms, i.e. cross-sections of the resonance set in four-dimensional parameter space. We also describe how the resonance set of the universal model is embedded in the bifurcation set by considering a corresponding approximating Takens normal form family of vector fields, compare with [6, 11].

Recovering the non-degenerate case. We first briefly reconsider the classical case of weak resonance, i.e. when $q \geqslant 5$. In this approach a planar universal diffeomorphism family is given by $P_\sigma : \mathbb{C} \to \mathbb{C}$, see [5, 7], determined by

$$P_\sigma(z) = \omega((1 + \sigma + |z|^2)z + \bar{z}^{q-1}) + O(|\sigma|^2, |z|^q) \tag{1}$$

(throughout we identify $\mathbb{R}^2$ with $\mathbb{C}$). Here ω is a primitive qth root of unity and $\sigma = \sigma_1 + i\sigma_2$ is a 'small' complex parameter. Our focus is on the q-periodic orbits of P_σ of which each point satisfies $P_\sigma^q(z) = z$. The number of these orbits changes at the boundary of the resonance set. Applying generalized Lyapunov–Schmidt reduction and $\mathbb{Z}_q$-equivariant contact-equivalence singularity theory, see [5], we obtain this boundary as the discriminant set of the real-valued polynomial $r_\sigma : \mathbb{R}_+ \to \mathbb{R}$ given by

$$r_\sigma(u) = |\sigma + u|^2 - u^{q-2}. \tag{2}$$

The number of local zeros of this polynomial equals the number of local q-periodic orbits of P_σ and the corresponding discriminant set is a $(q-2)/2$-cusp in the parameter plane given by

$$\sigma_2^2 = (-\sigma_1)^{q-2} + O(|\sigma_1|^{2q-4}). \tag{3}$$

Hence, our approach recovers that in this case the resonance set is the standard Arnol'd resonance tongue.

A study of the dynamics of P_σ is simplified by examining a Takens normal form vector field approximation [37] denoted by N_σ. The relation between P_σ and N_σ is given by

$$P_\sigma(z) = \Omega_{p/q} \circ N_\sigma^1(z) + O(|\sigma|^2, |z|^q), \tag{4}$$

Table 1. Relations between the dynamics of the universal family of the non-degenerate case P_σ and its Takens normal form vector field approximation N_σ. The transformation $\Omega_{p/q}$ is a rotation over $2\pi p/q$ around the origin.

P_σ	N_σ
Fixed point	Equilibrium
q-periodic orbit	q different equilibria invariant under $\Omega_{p/q}$
HNS bifurcation	Hopf bifurcation
Saddle-node bif. of q-periodic orbit	Saddle-node bif. of q different equilibria

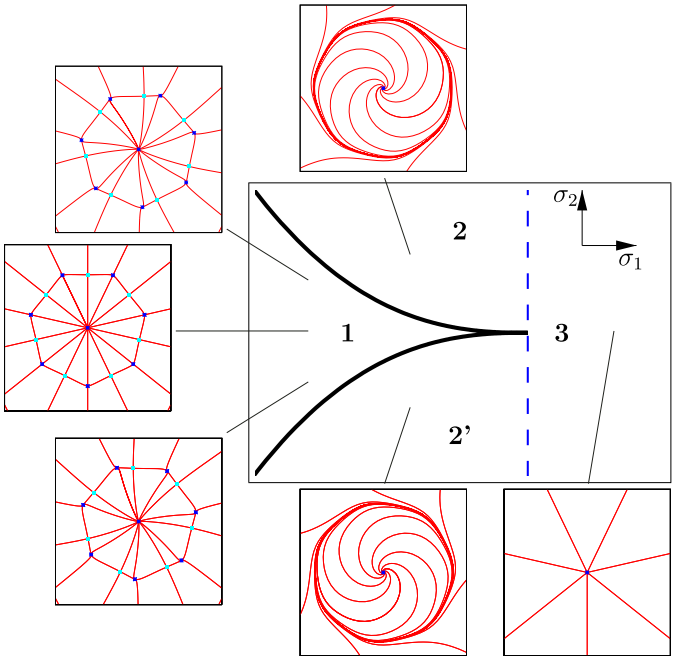

Figure 1. Bifurcation diagram of the Takens normal form vector field N_σ for the universal family of diffeomorphisms P_σ with $q = 7$. The bifurcation diagram contains a tongue shaped resonance set and a dashed Hopf-line.

where $\Omega_{p/q}$ is the rotation over $2\pi p/q$ around the origin, assuming $\omega = \mathrm{e}^{2\pi \mathrm{i} p/q}$ in (1) and N_σ^1 is the time-1-map of the flow of the vector field N_σ. As a consequence, the vector field family N_σ written as a map is of the form

$$N_\sigma(z) = (\sigma + |z|^2)z + \bar{z}^{q-1} + O(|\sigma|^2, |z|^q). \tag{5}$$

Since P_σ is approximated by the time-1-map of N_σ composed with a rotation, the dynamics of both families is closely related, see also table 1. The advantage of studying the approximating family of planar vector fields instead of the universal family of diffeomorphisms is that vector fields provide better visibility of the dynamics.

The bifurcation diagram of N_σ is presented in figure 1. Perturbation arguments, based on transversality theory, normally hyperbolic manifold theory and bifurcation theory [1, 16, 19, 23, 38], are used to recover the dynamics and bifurcations of P_σ, which are induced by those of N_σ. This is fully in line with the approach of, e.g. [6, 11, 22, 37]. Non-degenerate features of N_σ are expected to persist generically in P_σ, a list is given in table 1. We emphasize that all dynamical properties and bifurcations displayed in figure 1

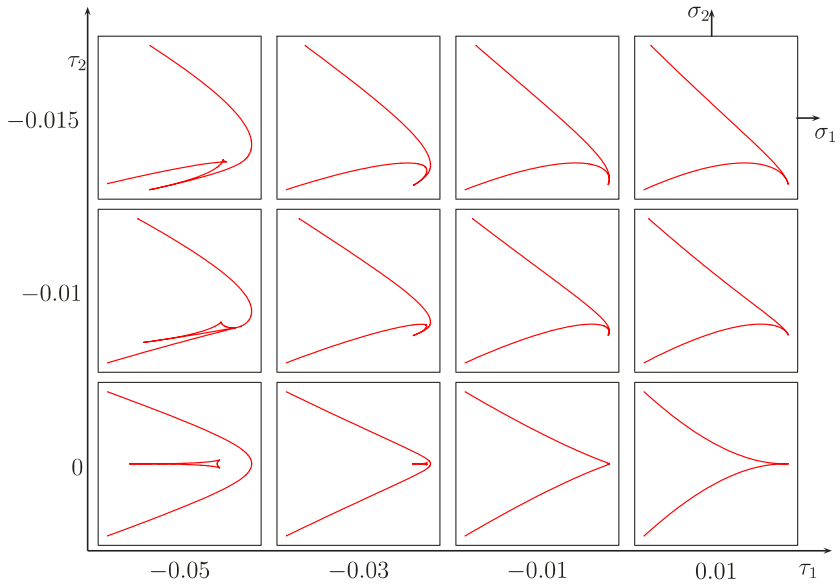

Figure 2. Several two-dimensional tomograms of the discriminant set of $p_{1,\sigma,\tau}$ for $q = 7$, compare with [5].

(and listed in table 1) are persistent under perturbations. Therefore, the bifurcation diagram of P_σ straightforwardly follows from figure 1: it consists of a curve of saddle-node bifurcations of periodic orbits and a line of HNS bifurcations of a fixed point.

Mildly degenerate resonance sets. The main focus of this paper is to understand the resonance set of the mildly degenerate universal diffeomorphism family $P_{\sigma,\tau} : \mathbb{C} \to \mathbb{C}$, see [5, 7], given by

$$P_{\sigma,\tau}(z) = \omega((1 + \sigma + \tau|z|^2 + |z|^4)z + \bar{z}^{q-1}) + O(|\sigma|^2, |\tau|^2, |z|^q), \tag{6}$$

where $\sigma = \sigma_1 + \mathrm{i}\sigma_2$ and $\tau = \tau_1 + \mathrm{i}\tau_2$ are 'small' complex parameters and ω is a primitive qth root of unity, with $q \geqslant 7$, assuming weak resonance. In this case we obtain the boundary of the resonance set as the discriminant set of the real-valued polynomial $p_{1,\sigma,\tau} : \mathbb{R}_+ \to \mathbb{R}$ given by

$$p_{1,\sigma,\tau}(u) = |\sigma + \tau u + u^2|^2 - u^{q-2}. \tag{7}$$

Again the number of local zeros of $p_{1,\sigma,\tau}$ corresponds to the number of local q-periodic orbits of $P_{\sigma,\tau}$. The discriminant set of $p_{1,\sigma,\tau}$ is analysed partially in [5] by providing a parametrization and an incomplete set of two-dimensional tomograms, similar to figure 2 (as in [5, figure 3], the value of $\tau = (\tau_1, \tau_2)$ is fixed in all two-dimensional tomograms of the resonance set presented in this paper).

As we presently show, the family $P_{\sigma,\tau}$ exhibits several other types of bifurcations beyond those of, e.g., saddle-node or cusp type belonging to the boundary of the resonance set. As above, the study of these additional bifurcations is here undertaken by the classical approach of examining a Takens normal form vector field approximation of the universal model $P_{\sigma,\tau}$, given by

$$N_{\sigma,\tau}(z) = z(\sigma + \tau|z|^2 + |z|^4) + \bar{z}^{q-1} + O(|\sigma|^2, |\tau|^2, |z|^q). \tag{8}$$

For this family we detect Hopf bifurcations, codimension 1 and 2 heteroclinic and homoclinic bifurcations of equilibria as well as codimension 2 degenerate Hopf and Bogdanov–Takens

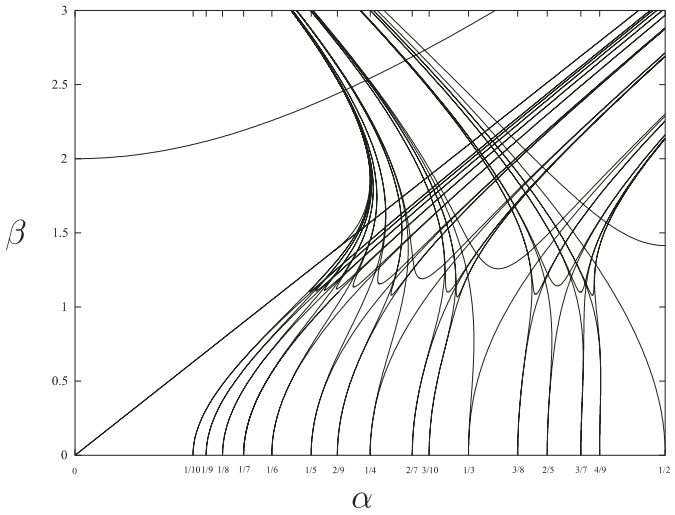

Figure 3. Resonance tongues in the Arnol'd family [8].

bifurcations. In this mildly degenerate case, all local features of the bifurcation diagram of $N_{\sigma,\tau}$ (including the local phenomena listed in table 1) generically translate directly into corresponding phenomena for $P_{\sigma,\tau}$. On the other hand, global phenomena such as heteroclinic and homoclinic bifurcations are generically expected to yield regions in parameter space characterized by tangles, i.e., transversal heteroclinic or homoclinic intersections of invariant manifolds [1, 19, 22, 23, 37].

Related work on resonance sets. In many applications, a family of planar diffeomorphisms is obtained from a family of vector fields by taking a suitable Poincaré map corresponding to a section transverse to a periodic orbit [5]. The eigenvalues of the derivative of the Poincaré map are the Floquet exponents of the periodic orbit. In particular, this approach also works for non-autonomous systems of differential equations depending periodically on time.

A toy model for the array of tongues of the HNS bifurcation is formed by the Arnol'd family of circle maps [1], given by $x \mapsto x + 2\pi\alpha + \beta \sin x$, where $x \in \mathbb{R}/(2\pi\mathbb{Z})$. Here in the (α, β)-plane tongues appear with their tips in $(\alpha, \beta) = (\frac{p}{q}, 0)$ and stretching out into the regions $\beta \neq 0$, see figure 3. The order of tangency of the tongue boundaries at the tip has the same asymptotics as in the HNS case, compare with [5, 6, 16]. For background regarding weak and strong resonances we refer to Takens [37], Newhouse *et al* [28], Arnol'd [1], Krauskopf [22] and Broer *et al* [5, 6, 12]. For resonance studied in Hamiltonian or reversible settings, etc see Broer and Vegter [11] or Vanderbauwhede [39]. For a study of dynamical features for parameter values 'far' from resonant HNS bifurcations, like the loss of smoothness of invariant circles, we refer to [2, 3, 10, 40].

The type of resonance mentioned in this paper is investigated before in [1, 9, 28, 37]. In general, these works study both the geometry of the resonance sets and the complete dynamics near resonance. On the other hand, the work of Broer *et al* [5–7], which is continued here, addresses the problem how to determine resonance sets in a general setting without being concerned with stability, other bifurcations and similar dynamical issues. The method used to solve this problem involves Lyapunov–Schmidt reduction opposed to the more often applied (Poincaré) normal form theory. It turns out that this approach simplifies studying more degenerate cases than those already investigated in earlier work [1, 9, 28, 37].

The research programme of Peckham *et al* reflected in [24, 25, 30–32] views resonance sets as projections on a 'traditional' parameter plane of saddle-node bifurcation sets in the product of parameter and phase space. This approach has the same spirit as ours and many interesting geometric properties of resonance sets are discovered and explained in this way.

In [13–15] Chenciner considers a 2-parameter unfolding of a degenerate HNS bifurcation. This bifurcation also appears in our study of the mildly degenerate case.

Outline of the paper. Section 2.1 contains a general description of Whitney stratifications. In particular, it is explained how to obtain such a stratification for a certain discriminant set. Section 2.2 presents the first main result, which is the Whitney stratification of the discriminant set of $p_{1,\sigma,\tau}$ given in (7). Section 3 contains our second main result, which consists of a bifurcation study of the Takens normal form family of vector fields $N_{\sigma,\tau}$ given in (8), compare with figure 1. Finally, all proofs of the theorems in section 2 are provided in appendix A.

2. Analysis of the resonance set

As mentioned above, we aim to improve our understanding of the geometry of the discriminant set of $p_{1,\sigma,\tau}$ defined in (7). We follow the catastrophe theory approach, which amounts to determining the corresponding Whitney stratification [4, 33]. The presentation of such a stratification usually involves providing parametrizations of the strata and showing several tomograms. Because of the complexity of the studied discriminant set, we extend such a presentation by displaying incidence relations between strata explicitly in incidence diagrams. Before actually providing the results (see section 2.2), we give a general definition of Whitney stratification in section 2.1, where we also indicate how to obtain such a stratification for a discriminant set.

2.1. Preliminaries

Whitney stratification. A stratification of a set $V \subset \mathbb{R}^n$ is a partition $\mathcal{X}$ of V into smooth path-connected submanifolds, called strata, such that (i) every point in V has a neighbourhood in $\mathbb{R}^n$ which meets only finitely many strata and (ii) if $X \cap \bar{Y} \neq \emptyset$ with $X, Y \in \mathcal{X}$, then $X \subset \bar{Y}$. We speak of a Whitney stratification if for all $x \in X \subset \bar{Y}$ with $X, Y \in \mathcal{X}$ and for all $y_i \in Y$ with $\lim_{i\to\infty} y_i = x$, the tangent space $T = \lim_{i\to\infty} T_{y_i}Y$ satisfies $T_xX \subset T$ [17]. A consequence of this condition is that a neighbourhood of every point on a particular stratum is homeomorphic to a neighbourhood of any other point on that stratum [18].

As an example we provide the Whitney stratification for the Whitney umbrella W [4], given by

$$W = \{(x, y, z) \in \mathbb{R}^3 \mid x^2y + z^2 = 0\}. \tag{9}$$

It is not hard to see that the Whitney stratification of W contains two codimension 1 surfaces, two codimension 2 half-lines and one codimension 3 point, where the Whitney umbrella is pinched, see figure 4.

Whitney stratification of a discriminant set. We start with the definition of a discriminant set of a family of polynomials $p_\mu(x)$, with $x \in \mathbb{R}$ and $\mu = (\mu_1, \ldots, \mu_n) \in \mathbb{R}^n$, a multiparameter. To this end we consider the manifold $M(p_\mu) = \{(x, \mu) \in \mathbb{R} \times \mathbb{R}^n \mid p_\mu(x) = 0\}$. The corresponding discriminant set $D(p_\mu)$ consists of the singular values of the natural projection $\pi : M(p_\mu) \to \mathbb{R}^n$, see [1]. This geometric point of view leads directly to the algebraic

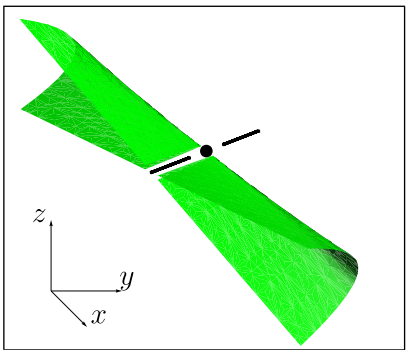

Figure 4. Whitney stratification of the Whitney umbrella W given in (9).

definition of the discriminant set $D(p_\mu)$ given by

$$D(p_\mu) = \left\{ \mu \in \mathbb{R}^n \mid p_\mu(x) = 0, \frac{\partial p_\mu}{\partial x}(x) = 0 \text{ for some } x \right\}. \tag{10}$$

It follows that the discriminant set is an algebraic set, i.e. it coincides with the zeros of a set of polynomials.

Strata of $D(p_\mu)$ are determined by parameter values for which the multiplicity of one zero of p_μ remains constant and is greater than 1 or by parameter values, where closures of strata intersect transversally. Firstly, the strata for which one zero, say x_0, has multiplicity $m > 1$ are of codimension $m-1$ and of type A_m [17], if (i) they are determined by the following system of equations,

$$\frac{\partial^j p_\mu}{\partial x^j}(x_0) = 0, \quad j = 0, \ldots, m-1 \qquad \text{and} \qquad \frac{\partial^m p_\mu}{\partial x^m}(x_0) \neq 0 \tag{11}$$

and (ii) for parameter values on these strata the following versality condition holds,

$$\operatorname{rank} \left[\frac{\partial \left(p_\mu, \dfrac{\partial p_\mu}{\partial x}, \ldots, \dfrac{\partial^{m-1} p_\mu}{\partial x^{m-1}} \right)}{\partial(\mu_1, \mu_2, \ldots, \mu_n)}(x_0) \right] = m - 1. \tag{12}$$

Conditions (11) and (12) are called recognition conditions for strata of type A_m. We note that strata of discriminant sets are semi-algebraic sets, because they are determined by a set of polynomial equations and inequalities. Secondly, if closures of strata intersect transversally, then the intersection points form a stratum of codimension equal to the sum of the codimensions of the 'intersecting' strata. As usual, the set of intersection points of, e.g., closures of strata of type A_m and A_n is denoted by $A_m A_n$ if $m \neq n$ and by A_m^2 if $m = n$. To distinguish different strata of the same type, we add an extra subscript to the corresponding labels, see, e.g. figure 5.

We illustrate the above in figure 5 for $p_{a,b}(x) = x^3 + ax + b$, with x, a and b real, yielding a singularity of type A_3, i.e. the standard cusp [33]. More precisely, figure 5 depicts the two-dimensional manifold $M(p_{a,b})$ and points for which $\pi : M(p_{a,b}) \mapsto \{(a,b) | a, b \in \mathbb{R}\}$ is singular. By definition the image of these points under the projection π is $D(p_{a,b})$. The corresponding Whitney stratification consists of a stratum of type A_3 and of two strata of type A_2, which are given by the image under the projection π of the points where $M(p_{a,b})$ folds. Figure 5 also depicts the incidence diagram of $D(p_{a,b})$. Similarly, the set $D(r_\sigma)$ with r_σ as in (2) yields the boundary of the standard Arnol'd tongue. The corresponding Whitney

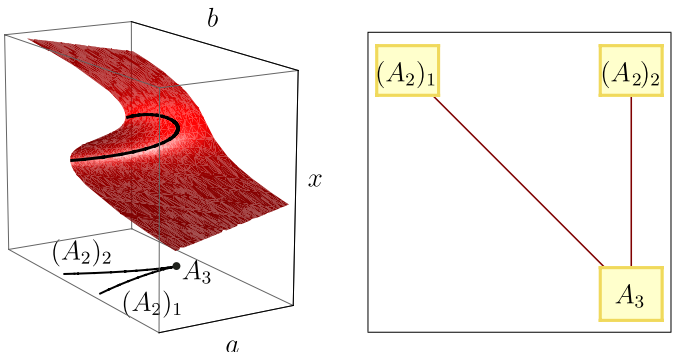

Figure 5. Discriminant set of $p_{a,b}(x) = x^3 + ax + b$ and the corresponding incidence diagram. The set $D(p_{a,b})$, containing strata of type A_2 and A_3, is determined by the singular values of $\pi : M(p_{a,b}) \to \{(a, b)|a, b \in \mathbb{R}\}$.

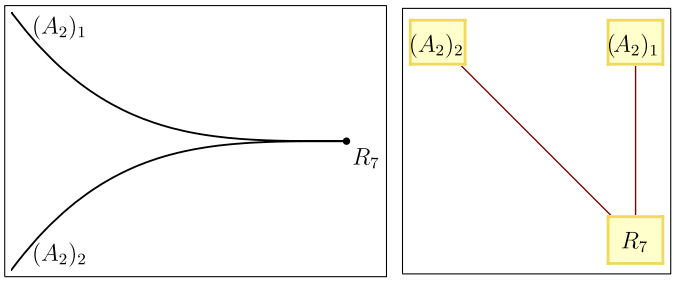

Figure 6. Arnol'd tongue for $q = 7$ and the corresponding incidence diagram, compare with figure 1.

stratification is provided in figure 6. As in this figure, from now on we refer to the central singularity of $D(r_\sigma)$ as a singularity of type R_q. Also for $D(p_{1,\sigma,\tau})$ with $p_{1,\sigma,\tau}$ as in (7) we can determine the stratification. Below we show that strata of codimension 1 up to and including 4 appear, which are usually named after their local geometry, see table 2.

Remark 2.1.

(1) The labels used for fold, cusp and swallowtail singularities are standard in catastrophe theory [17, 33, 38].
(2) For obvious reasons, we label the central singularities of the resonance sets encountered in this paper with R_q and we add a hat to refer to the mildly degenerate case. To explain the geometry of $D(p_{1,\sigma,\tau})$ we consider a closely related set below in section 2.2, whose central singularity does not depend on q and is therefore labelled with $\hat{R}_\infty$.
(3) We apply a catastrophe theory approach to study the discriminant set of a real polynomial, compare with [33]. Usually, this polynomial depends on an unrestricted variable, as in the example of the singularity of type A_3, where $p_{a,b}$ depends on $x \in \mathbb{R}$. However, the polynomials r_σ and $p_{1,\sigma,\tau}$ depend on $u \in \mathbb{R}_+$, leading to extra strata for $u = 0$, which might not be there if $u \in \mathbb{R}$. We say these extra strata are of boundary type, since they are always part of the boundary of another stratum. They are labelled by prefixing a ∂ to the type of stratum of which they form a part of the boundary. An exception to this are the labels R_q, $\hat{R}_q$ and $\hat{R}_\infty$, which are in fact also of boundary type.

Table 2. Codimensions and names of strata of a particular type. The pinch point appeared already in the Whitney umbrella (9) and the collapsed mildly degenerate resonance set is introduced in section 2.2. For more explanation on use of labels we refer to remark 2.1.

Cod.	Type	
1	A_2	(fold)
2	A_3	(cusp)
2	R_q	(central singularity of non-degenerate Arnol'd resonance tongue)
3	A_4	(swallowtail)
3	P	(pinch point)
4	$\hat{R}_\infty$	(central singularity of collapsed mildly degenerate resonance set)
4	$\hat{R}_q$	(central singularity of q-dependent mildly degenerate resonance set)
m	∂A_m	(stratum of boundary type)

(4) We keep each graph with incidence relations clear by only displaying relations between strata that differ by 1 in codimension, see figures 8 and 10. In this case, the incidence diagram is determined by the corresponding transitive closure, which extends the depicted graph G with edges between pairs of vertices that (i) correspond to strata that differ by $m > 1$ in codimension and that (ii) are joined by a path of length m in G.

2.2. *Geometry and incidence relations of* $D(p_{1,\sigma,\tau})$

The geometry of $D(p_{1,\sigma,\tau})$ is complicated. However, the polynomial $p_{1,\sigma,\tau}$ given in (7) can be regarded as a 'singular perturbation' of the polynomial $p_{0,\sigma,\tau} : \mathbb{R}_+ \to \mathbb{R}$ given by

$$p_{0,\sigma,\tau}(u) = |\sigma + \tau u + u^2|^2, \tag{13}$$

which has a simpler discriminant set $D(p_{0,\sigma,\tau})$. In fact, $D(p_{1,\sigma,\tau})$ can be scaled to a neighbourhood of $D(p_{0,\sigma,\tau})$ as follows.

Relation between $D(p_{1,\sigma,\tau})$ *and* $D(p_{0,\sigma,\tau})$. We relate $p_{1,\sigma,\tau}$ and $p_{0,\sigma,\tau}$ by a scaling $\phi_\varepsilon : \mathbb{R}_+ \times \mathbb{C}^2 \to \mathbb{R}_+ \times \mathbb{C}^2$ given by

$$\phi_\varepsilon : (u, \sigma, \tau) \mapsto (\varepsilon u, \varepsilon\sigma, \varepsilon^2\tau), \tag{14}$$

with $\varepsilon \in \mathbb{R}_+$. Using the notation $p_\star(u, \sigma, \tau) = p_{\star,\sigma,\tau}(u)$ and defining $p_\varepsilon = \varepsilon^{-4} p_1 \circ \phi_\varepsilon$, we obtain $p_{\varepsilon,\sigma,\tau} : \mathbb{R}_+ \to \mathbb{R}$ given by

$$p_{\varepsilon,\sigma,\tau}(u) = |\sigma + \tau u + u^2|^2 - \varepsilon^{q-6} u^{q-2}, \tag{15}$$

which 'interpolates' between $p_{1,\sigma,\tau}$ and $p_{0,\sigma,\tau}$. It follows that $D(p_{\varepsilon,\sigma,\tau})$ for $\varepsilon \neq 0$ is diffeomorphic to $D(p_{1,\sigma,\tau})$ by the scaling ϕ_ε. Moreover, the set $D(p_{\varepsilon,\sigma,\tau})$ for $\varepsilon \neq 0$ is a singular perturbation of the 'geometric centre' $D(p_{0,\sigma,\tau})$, as is illustrated in figure 7. More precisely, considering the Hausdorff metric [27] d_H given by

$$d_H(X, Y) = \max\{\sup_{x\in X} \inf_{y\in Y} d(x, y), \sup_{y\in Y} \inf_{x\in X} d(x, y)\}, \tag{16}$$

where $X, Y \subset \mathbb{R}^n$ are bounded and d is the Euclidean metric, we obtain

$$d_H(D(p_{\varepsilon,\sigma,\tau}), D(p_{0,\sigma,\tau})) = O(\varepsilon^{(q-6)/2}),$$

see appendix A.1.

A useful property of $p_{\varepsilon,\sigma,\tau}$ and $D(p_{\varepsilon,\sigma,\tau})$ is that they have a $\mathbb{Z}_2$-symmetry, since they are invariant under the involution $t : \mathbb{R}^4 \to \mathbb{R}^4$ given by

$$t(\sigma_1, \sigma_2, \tau_1, \tau_2) = (\sigma_1, -\sigma_2, \tau_1, -\tau_2). \tag{17}$$

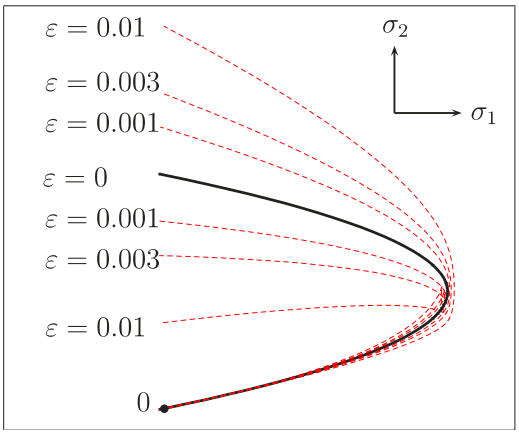

Figure 7. A two-dimensional tomogram of $D(p_{\varepsilon,\sigma,\tau})$ for $\tau = (-0.1, 0.005)$ and varying ε.

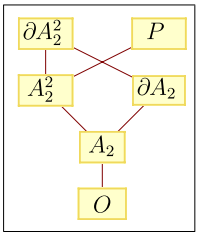

Figure 8. Graph generating the incidence diagram of $D(p_{0,\sigma,\tau})$ by taking the transitive closure. The top row gives the codimension 3 strata, the second the codimension 2 strata and the third the codimension 1 stratum. Moreover, the set O is the only connected open region in $\mathbb{R}^4$. The central singularity is omitted, since it is incident to all other strata.

Whitney stratification of $D(p_{0,\sigma,\tau})$. We continue with an analysis of $D(p_{0,\sigma,\tau})$, which already demonstrates several features of $D(p_{\varepsilon,\sigma,\tau})$ for $\varepsilon \neq 0$.

Theorem 2.1 (Whitney stratification of $D(p_{0,\sigma,\tau})$**).** *An implicit representation of* $D(p_{0,\sigma,\tau})$ *is given by*

$$\{(\tau_1, \tau_2, \sigma_1, \sigma_2) \in \mathbb{R}^4 \mid \tau_2^2\sigma_1 - \tau_1\tau_2\sigma_2 + \sigma_2^2 = 0,\ \operatorname{sign}(\sigma_2) = -\operatorname{sign}(\tau_2)\},$$

which is diffeomorphic to a subset of the product of the real line and the Whitney umbrella W. *The set* $D(p_{0,\sigma,\tau})$ *contains the following strata.*

cod.1 *One codimension* 1 *stratum of type* A_2.
cod.2 *Two codimension* 2 *strata of type* A_2^2 *and* ∂A_2.
cod.3 *Two codimension* 3 *strata of type* ∂A_2^2 *and* P. *Both strata only occur for* $\tau_1 < 0$.
cod.4 *The codimension* 4 *stratum of type* $\hat{R}_\infty$, *which is the central singularity situated at* $(\sigma, \tau) = (0, 0)$.

The incidence diagram of $D(p_{0,\sigma,\tau})$ *is the transitive closure of the graph displayed in figure 8.*

For a proof see appendix A.2.

The stratification provided in theorem 2.1 is illustrated by three-dimensional tomograms of $D(p_{0,\sigma,\tau})$, see figure 9. As in this figure, the value of τ_1 is constant for every three-dimensional tomogram of $D(p_{\varepsilon,\sigma,\tau})$ displayed in this paper (mostly the value $\tau_1 = -0.1$

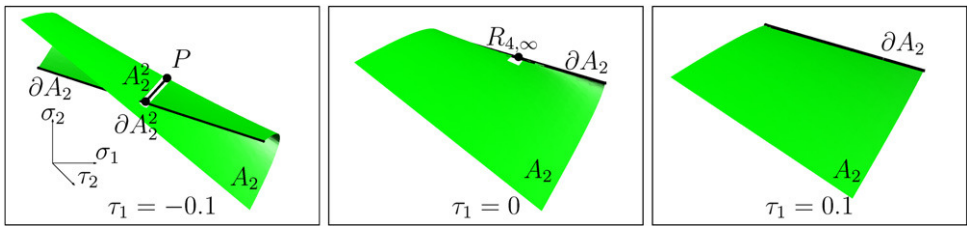

Figure 9. Three three-dimensional tomograms of $D(p_{0,\sigma,\tau})$ showing its Whitney stratification for $-0.02 \leqslant \tau_2 \leqslant 0.02$.

is used). In appendix A.5 it is shown that any three-dimensional tomogram of $D(p_{0,\sigma,\tau})$ is diffeomorphic to one of the tomograms depicted in figure 9. The relation between the Whitney umbrella and $D(p_{0,\sigma,\tau})$ is clarified by comparing figures 4 and 9.

Whitney stratification of $D(p_{\varepsilon,\sigma,\tau})$ for $\varepsilon \neq 0$. Now we present the Whitney stratification of $D(p_{\varepsilon,\sigma,\tau})$ for $\varepsilon \neq 0$.

Theorem 2.2 (Whitney stratification of $D(p_{\varepsilon,\sigma,\tau})$ for $\varepsilon \neq 0$). *Consider the stratification of $D(p_{0,\sigma,\tau})$, see theorem 2.1. In general, the set $D(p_{\varepsilon,\sigma,\tau})$ is in an $O(\varepsilon^{(q-6)/2})$-neighbourhood of $D(p_{0,\sigma,\tau})$ in the Hausdorff metric. In particular, for the strata of $D(p_{\varepsilon,\sigma,\tau})$ we have the following.*

cod.1 *The five strata labelled with $(A_2)_1$, $(A_2)_2$, $(A_2)_3$, $(A_2)_4$ and $(A_2)_5$ are in an $O(\varepsilon^{(q-6)/2})$-neighbourhood of the stratum of type A_2 of $D(p_{0,\sigma,\tau})$.*

cod.2 *The stratum labelled with R_q coincides with the stratum of type ∂A_2 of $D(p_{0,\sigma,\tau})$. The two pairs of strata labelled with $(A_2^2)_1^{\pm}$ and $(A_2^2)_2^{\pm}$ are in an $O(\varepsilon^{(q-6)/4})$-neighbourhood and an $O(\varepsilon^{(q-6)/2})$-neighbourhood respectively of the stratum of type A_2^2 of $D(p_{0,\sigma,\tau})$. Finally, the two pairs of strata labelled with $(A_3)_1^{\pm}$ and $(A_3)_2^{\pm}$ are in an $O(\varepsilon^{(q-6)/4})$-neighbourhood of the stratum P of $D(p_{0,\sigma,\tau})$.*

cod.3 *The pair of strata labelled with $(R_q A_2)^{\pm}$ is in an $O(\varepsilon^{(q-6)/2})$-neighbourhood of the stratum of type ∂A_2^2 of $D(p_{0,\sigma,\tau})$. The two pairs of strata labelled with $(A_4)_1^{\pm}$ and $(A_4)_2^{\pm}$ are in an $O(\varepsilon^{(q-6)/2})$-neighbourhood and an $O(\varepsilon^{(q-6)/4})$-neighbourhood respectively of the stratum of type P of $D(p_{0,\sigma,\tau})$. Also for $\varepsilon \neq 0$ all codimension 3 strata only occur for $\tau_1 < 0$.*

cod.4 *The central singularity, which is of type $\hat{R}_q$ coincides with the central singularity of type $\hat{R}_\infty$ of $D(p_{0,\sigma,\tau})$.*

For $\varepsilon \neq 0$ the set $D(p_{\varepsilon,\sigma,\tau})$ separates the neighbourhood of $(\sigma, \tau) = (0, 0)$ in the 3 connected open regions O_1, O_2 and O_3, for which the polynomial $p_{\varepsilon,\sigma,\tau}$ given in (7), has zero, two and four local zeros, respectively.

The incidence diagram of $D(p_{\varepsilon,\sigma,\tau})$ for $\varepsilon \neq 0$ is the transitive closure of the graph displayed in figure 10.

For a proof see appendices A.3 and A.4. We note that theorem 2.2 is valid for all $q \geqslant 7$, not only for $q = 7$, which is used in the figures.

The $\mathbb{Z}_2$-symmetry of $D(p_{\varepsilon,\sigma,\tau})$ for $\varepsilon \neq 0$ implies that several strata are similar. More precisely, the map t as defined in (17) transforms every superscript plus in a superscript minus and vice versa, for instance $t((A_4)_1^{\pm}) = (A_4)_1^{\mp}$. There is one exception, namely $t((A_3)_1^{\pm}) = (A_3)_2^{\mp}$. The strata labelled without superscript are invariant under t.

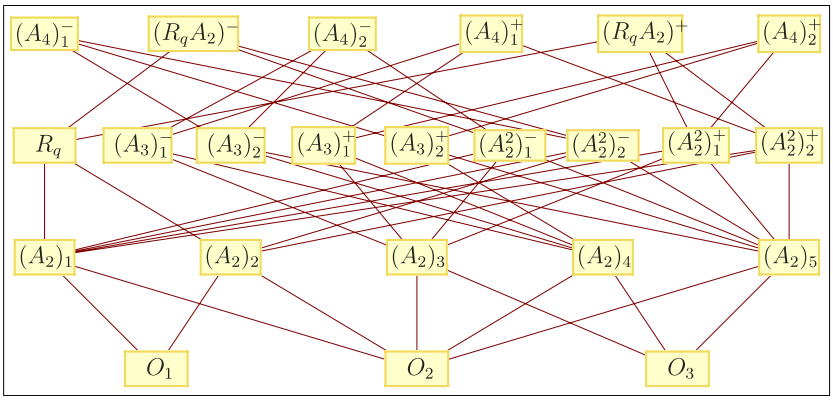

Figure 10. Graph generating the incidence diagram of $D(p_{\varepsilon,\sigma,\tau})$ for $\varepsilon \neq 0$ by taking the transitive closure. The top row gives the codimension 3 strata, the second the codimension 2 strata and the third the codimension 1 strata. The bottom row gives all connected open components in the neighbourhood of $(\sigma, \tau) = (0, 0)$. The central singularity is omitted, since it is incident to all other strata.

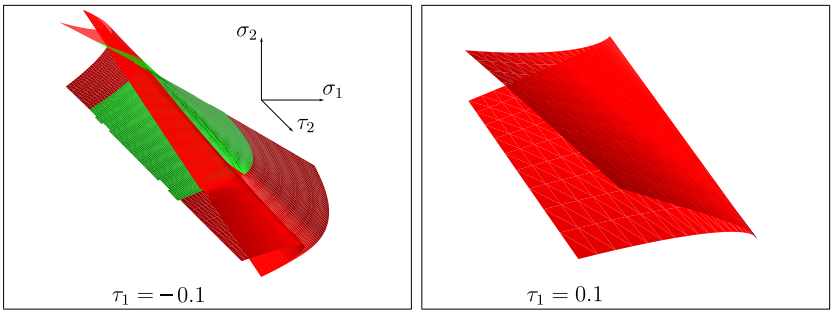

Figure 11. Two generic three-dimensional tomograms of $D(p_{1,\sigma,\tau})$ for $-0.02 \leqslant \tau_2 \leqslant 0.02$ and $q = 7$. There are two shadings, if the corresponding two-dimensional tomogram with fixed τ has two disconnected components.

Two generic three-dimensional tomograms of $D(p_{1,\sigma,\tau})$ are displayed in figure 11. Indeed, appendix A.5 shows that any generic three-dimensional tomogram of $D(p_{1,\sigma,\tau})$ is diffeomorphic to one of the tomograms in figure 11. The features of the three-dimensional tomogram for $\tau_1 < 0$ are hard to distinguish; hence, we include figures 12 and 13 that zoom in on the more interesting parts of this tomogram. Because of the $\mathbb{Z}_2$-symmetry, we may restrict to the case $\tau_2 < 0$. To be precise, figure 12 depicts the geometry near the codimension 3 strata $(A_4)_1^-$ and $(R_7A_2)^-$ and figure 13 depicts the geometry near the codimension 3 stratum $(A_4)_2^-$. The relation between figures 12(a) and 13(a) is that by decreasing τ_2 the first continues into the latter, which can be read off from the τ_2-values for both plots. A consequence is that the two-dimensional tomogram, which follows in figure 12(g) is figure 13(b). For clarity, the standard geometry near a point of a stratum of type A_4 is depicted in figure 14.

Finally, figure 15 presents all possible types of two-dimensional tomograms around $\tau = 0$, compare with figure 2. The top panel in figure 15 indicates the τ-values for which the geometry of the tomograms changes. In appendix A.5 it is shown that these values correspond to the projections on the τ-plane of all codimension 3 strata and of the curves $T^{\pm}$. The curves $T^{\pm}$ are given by the parameter values for which a two-dimensional tomogram with fixed τ is tangent

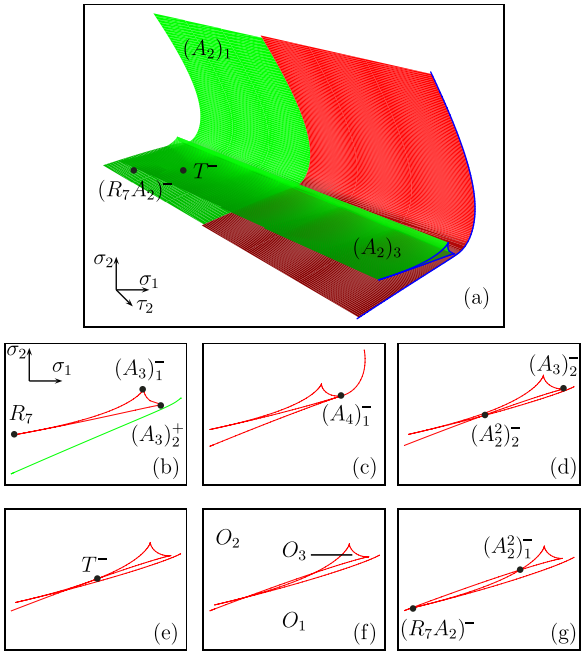

Figure 12. A three-dimensional tomogram of $D(p_{1,\sigma,\tau})$ for $q = 7$, $\tau_1 = -0.1$ and $-0.011 \leqslant \tau_2 \leqslant -0.006$. Figures (*b*)–(*g*) give the corresponding two-dimensional tomograms for decreasing values of τ_2. There are two shadings if the corresponding two-dimensional tomogram with τ fixed has two disconnected components. At a point on T^- a two-dimensional cross-section of (σ, τ)-parameter space is tangent to $(A_2^2)_1^-$. The importance of these points is discussed at the end of section 2.2 and in appendix A.5.

to $(A_2^2)_1^+$ or $(A_2^2)_1^-$, respectively. Hence, these curves are not strata in the Whitney stratification, so they do not correspond to an extra type of bifurcation of $P_{\sigma,\tau}$ given in (6).

3. Bifurcation diagram of a Takens normal form approximation

The analysis of the resonance set of $P_{\sigma,\tau}$ is now extended by a numerical bifurcation study for a Takens approximating family of vector fields $N_{\sigma,\tau}$. This study is contained in sections 3.1–3.3 and is followed by a discussion of the features, which are expected to persist in the universal family $P_{\sigma,\tau}$ (section 3.4).

The Takens approximating family is derived in analogy with the non-degenerate case presented in the introduction (see (4)):

$$P_{\sigma,\tau}(z) = \Omega_{p/q} \circ N^1_{\sigma,\tau}(z) + O(|\sigma|^2, |\tau|^2, |z|^q), \tag{18}$$

where $z = x + \mathrm{i}y$, $\sigma = \sigma_1 + \mathrm{i}\sigma_2$ and $\tau = \tau_1 + \mathrm{i}\tau_2$ are 'small' complex numbers, $\Omega_{p/q}$ is the rotation over $2\pi p/q$ around the origin and $N^1_{\sigma,\tau}$ is the time-1-map of $N_{\sigma,\tau}$. For $q = 7$, taking $\omega = \exp(2\pi\mathrm{i}/7)$ in (6) yields

$$N_{\sigma,\tau}(z) = z(\sigma + \tau|z|^2 + |z|^4) + \bar{z}^6 + O(|\sigma|^2, |\tau|^2, |z|^7). \tag{19}$$

Exploration of the bifurcation set by two-dimensional tomograms. A full study of the four-dimensional parameter space of $N_{\sigma,\tau}$ would be too cumbersome, due to the large number of bifurcations occurring. We restrict to selected two-dimensional tomograms (obtained with τ

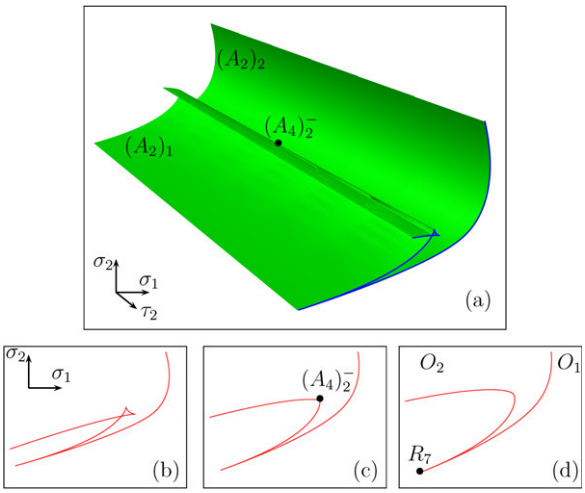

Figure 13. A three-dimensional tomogram of $D(p_{1,\sigma,\tau})$ for $q = 7$, $\tau_1 = -0.1$ and $-0.02 \leqslant \tau_2 \leqslant -0.011$. In the figures (*b*)–(*d*) the corresponding two-dimensional tomograms are given for decreasing fixed values of τ_2. (*b*) shows a wedge shaped region with vertices that are points from the strata $(A_2^2)_1^-$, $(A_3)_1^-$ and $(A_3)_2^-$ and edges that are points from the strata $(A_2)_3$, $(A_2)_4$ and $(A_2)_5$, see also figure 12. Points inside the wedge area belong to O_3. For comparison, the standard geometry near a point of type A_4 is given in figure 14.

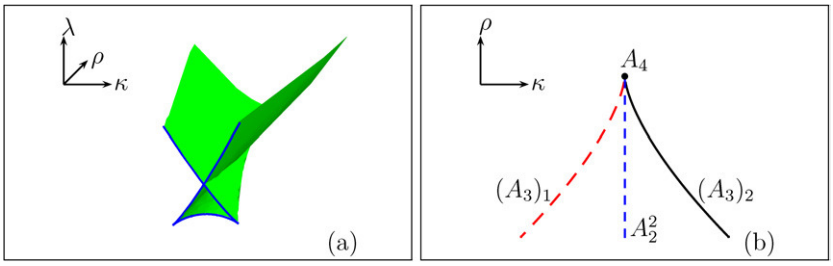

Figure 14. Standard geometry near a point of type A_4. This geometry is locally diffeomorphic to the geometry of $D(p_{1,\sigma,\tau})$ near points of type A_4, see figures 12 and 13. The transformation relating (ρ, κ, λ)-coordinates and $(\sigma_1, \sigma_2, \tau_2)$-coordinates is provided in appendix A.4. (*b*) shows the projections of codimension 2 and 3 strata in figure (*a*) on the (κ, ρ)-plane.

fixed) that do not contain codimension 3 and 4 bifurcations. More specifically, we aim to recover generic tomograms of the resonance set by considering τ-values that are separated by projections of codimension 3 strata on the τ-plane, see figure 15. By the results of section 2.2, we focus on the following three cases.

(1) The parameter τ between the τ-plane projections of $(A_4)_1^+$ and $(A_4)_1^-$: the two-dimensional tomograms of the resonance set consist of two disconnected parts, a detached 'swallowtail' (i.e. the wedge shaped region) and a stratum of type A_2, see figure 15(*a*). A representative tomogram with $\tau = (-0.1, 0)$ is analysed in section 3.1.

(2) The parameter τ between the τ-plane projections of $(A_4)_1^-$ and $(A_4)_2^-$: the two-dimensional tomograms of the resonance set consist of one connected part which also contains a 'swallowtail', see figure 15(*c*). A representative tomogram with $\tau = (-0.1, -0.0339)$ is analysed in section 3.2. By the $\mathbb{Z}_2$-symmetry in (17) this also represents tomograms with τ-values between projections of $(A_4)_1^+$ and $(A_4)_2^+$.

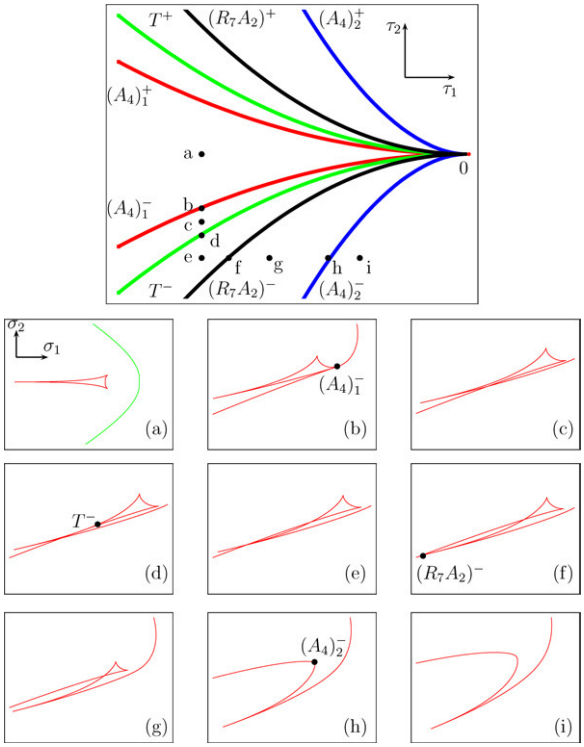

Figure 15. Overview of two-dimensional tomograms of $D(p_{1,\sigma,\tau})$ for $q = 7$, compare with figures 12 and 13. The top panel contains a sketch of the τ-values for which the geometry of two-dimensional tomograms changes. These values are given by the projections of $(A_4)_1^{\pm}$, $(A_4)_2^{\pm}$, $T^{\pm}$ and $(R_7A_2)^{\pm}$ on the τ-plane, see appendix A.5.

(3) The parameter τ 'outside' the τ-plane projections of $(A_4)_2^+$ and $(A_4)_2^-$: the two-dimensional tomograms of the resonance set consist of one connected cusp-shaped part, see figure 15(i). A representative tomogram with $\tau = (-0.1, -0.056)$ is analysed in section 3.3.

Remark 3.1.

(1) Within each tomogram the parameters σ_1 and σ_2 are used for the bifurcation study of $N_{\sigma,\tau}$, while τ_1 is fixed throughout.
(2) Since the τ-values are chosen not to coincide with strata of codimension 3 or higher, only strata of type A_2 and A_3 are found in the tomograms. These strata are labelled consistently with section 2.2.
(3) The τ-plane region between curves $T^{\pm}$ and $(R_7A_2)^{\pm}$ is not explored, because it does not contain more types of codimension 1 and 2 bifurcations than those obtained in sections 3.1, 3.2 and 3.3.
(4) The numerical methods of [36] are used for the continuation of bifurcations and for the computation of invariant manifolds. The Taylor integrator of [21] is used to compute the flow of the vector field $N_{\sigma,\tau}$.
(5) By [23] the central equilibrium of $N_{\sigma,\tau}$ undergoes a non-degenerate Hopf bifurcation for $\sigma_1 = 0$ if $\sigma_2 \neq 0$ and $\tau_1 \neq 0$. This bifurcation is supercritical (subcritical) if τ_1 is negative (positive). Degenerate Hopf bifurcations [23] occur for $(\sigma_1, \tau_1) = (0, 0)$ and $\sigma_2 \neq 0$. By the results of section 2, the mildly degenerate resonance set is attached to this set of codimension 2 bifurcations.

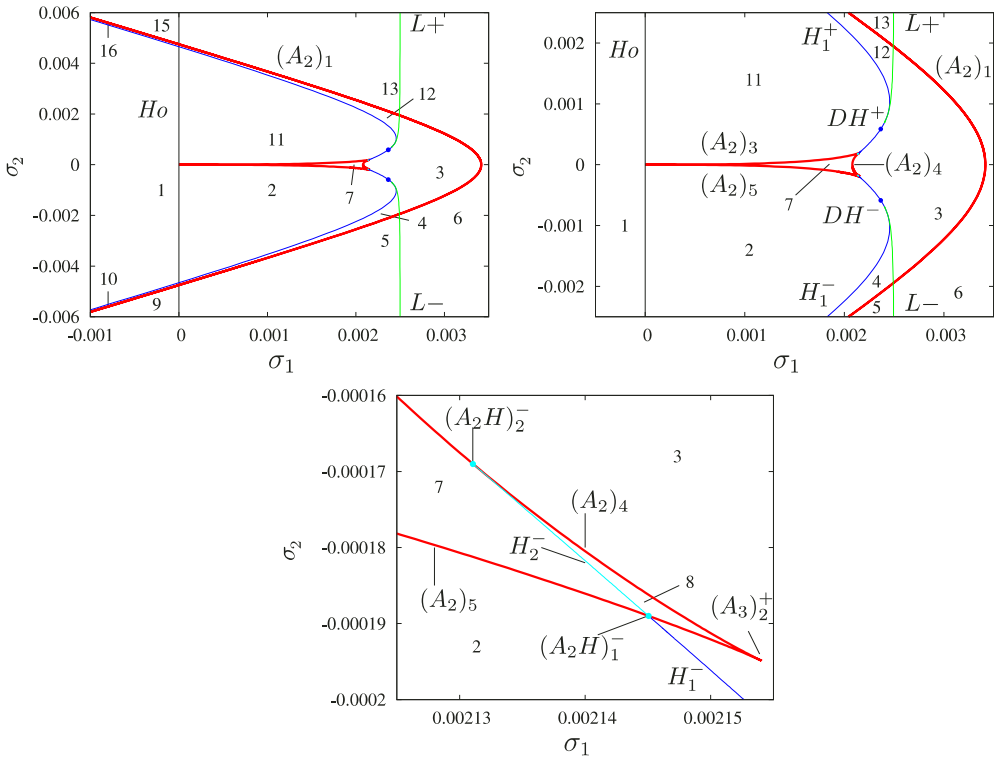

Figure 16. Bifurcation set of the planar Takens normal form vector field $N_{\sigma,\tau}$ given in (19) for $\tau = (-0.1, 0)$, with two subsequent magnifications in the σ-parameter plane near interesting regions, see section 3.1 for the meaning of the symbols. The curves of type A_2 are fatter to facilitate identification of the resonance set as illustrated in figure 15(*a*).

(6) In [7] the universal families P_σ as in (1) and $P_{\sigma,\tau}$ as in (6) are obtained by applying $\mathbb{Z}_q$-equivariant contact-equivalences. These transformations, which do not preserve stability, allow all constant non-zero coefficients to be scaled to 1 in P_σ and $P_{\sigma,\tau}$. By (4) and (18) the same holds for the corresponding Takens normal form families. On the other hand, if normalizing transformations are used that do preserve stability, not all constant coefficients can be scaled to 1, see, e.g. [13].

3.1. Tomogram with detached swallowtail

We now extend the two-dimensional tomogram of the resonance set in figure 15(*a*). For $\tau = (-0.1, 0)$ the vector field $N_{\sigma,\tau}$ possesses the extra $\mathbb{Z}_2$-symmetry generated by

$$\sigma_2 \mapsto -\sigma_2, \qquad y \mapsto -y, \tag{20}$$

which is used to simplify the presentation of the corresponding bifurcation diagram.

Strata in the bifurcation set. The bifurcation set displayed in figure 16 contains the following curves.

(1) A curve *Ho* of Hopf bifurcations.
(2) Curves of saddle-node bifurcations of equilibria corresponding to strata of type A_2 in the resonance set.

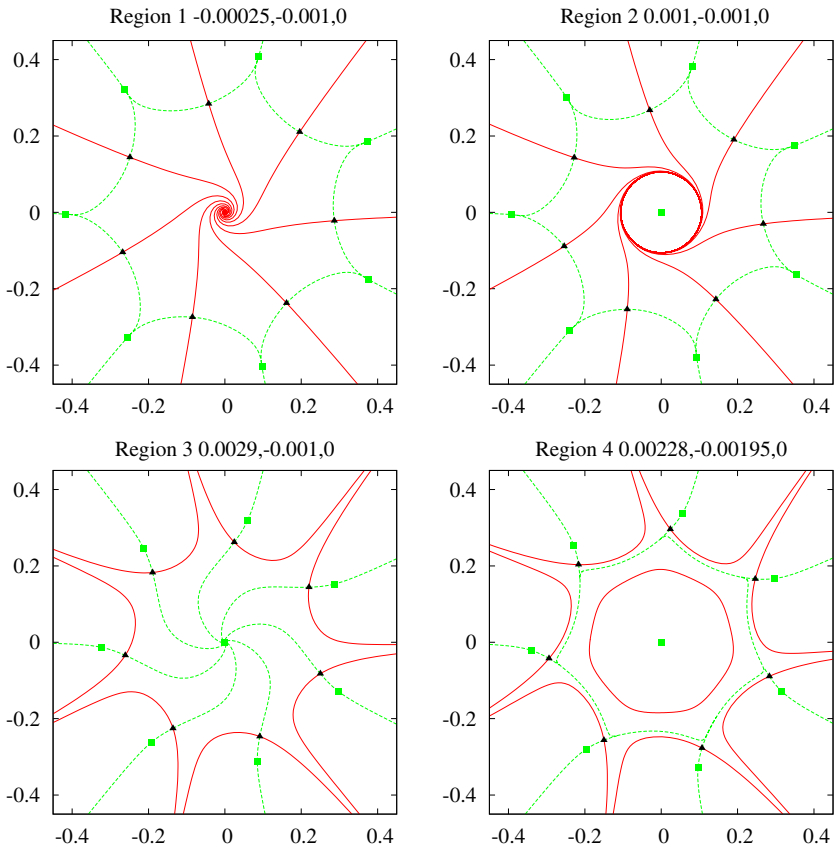

Figure 17. Phase portraits of the Takens normal form vector field $N_{\sigma,\tau}$ in (19). The top of each plot shows the region in the parameter plane (see figure 16) and the values of σ_1, σ_2 and τ_2.

(3) Two curves $L^{\pm}$ of saddle-node bifurcations of limit cycles.
(4) Four curves $H^{\pm}_{1,2}$ of heteroclinic bifurcations of equilibria (see below for a definition).

Moreover, the following codimension 2 bifurcation points occur.

(1) Two cusp bifurcations of equilibria corresponding to the strata $(A_3)^-_1$ and $(A_3)^+_2$ in the resonance set.
(2) Two points $DH^{\pm}$ of degenerate heteroclinic bifurcations of equilibria.
(3) Four points $(A_2H)^{\pm}_{1,2}$ of degenerate heteroclinic bifurcations of equilibria.

The curves $L^{\pm}$ are tangent to the curves $H^{\pm}_1$ at the points $DH^{\pm}$, respectively (figure 16, top right panel). The curve H^-_1 terminates at the point $(A_2H)^-_1$ on the saddle-node curve $(A_2)_5$ with a *transversal* intersection (figure 16, bottom panel). The curve H^-_2 is contained in the interior of the wedge and joins the points $(A_2H)^-_1$ and $(A_2H)^-_2$. Note that H^-_2 is tangent to $(A_2)_4$ and transversal to $(A_2)_5$. We stress that the point $(A_2H)^-_1$ is a codimension 2 bifurcation (see below) and is not just a projection-induced overlap. A symmetric configuration is found in the upper half of the σ-parameter plane.

The above curves induce a subdivision of the parameter plane in 16 regions characterized by topologically equivalent phase portraits. We only present phase portraits for regions 1–10 (see figures 17, 18 and 19). Due to (20), phase portraits for regions 11 to 16 are symmetric to

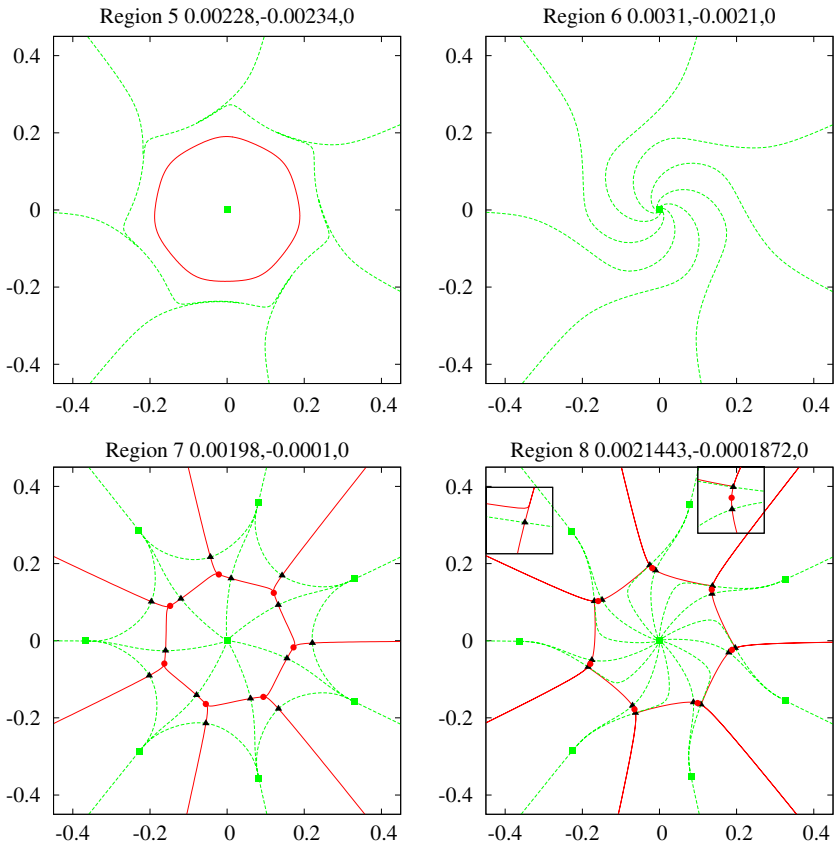

Figure 18. Continuation of figure 17. For region 8, two subsequent magnifications near one of the saddles have been added in the boxes.

those for regions 2, 4, 5, 8, 9, 10. For this reason, only the lower half of the parameter plane is discussed here.

Remark 3.2.

(1) Equilibria invariant under $\Omega_{1/7}$, which generates a $\mathbb{Z}_7$-symmetry, are from here on referred to as $\mathbb{Z}_7$-symmetric equilibria.
(2) In the phase portraits, attracting (repelling) periodic orbits are represented by solid (dashed) curves. Coherently, unstable (stable) manifolds of saddle equilibria are solid (dashed) curves. Equilibria are plotted with different shapes according to their stability type: attractors, repellors and saddles are plotted with small discs, squares and triangles, respectively.
(3) Seven branches of unstable manifolds appear in figures 18 and 19, coming from *outside* of the plotted region. These are due to a family of $\mathbb{Z}_7$-symmetric equilibria located outside of the neighbourhood of the origin of our present interest. The bifurcations induced by these saddles are not included in this study.

A neighbourhood of the origin consists of the four regions 1, 2, 7 and 11. Here a repelling invariant limit cycle exists, which is phase-locked in a $1:7$-resonance. It consists of seven

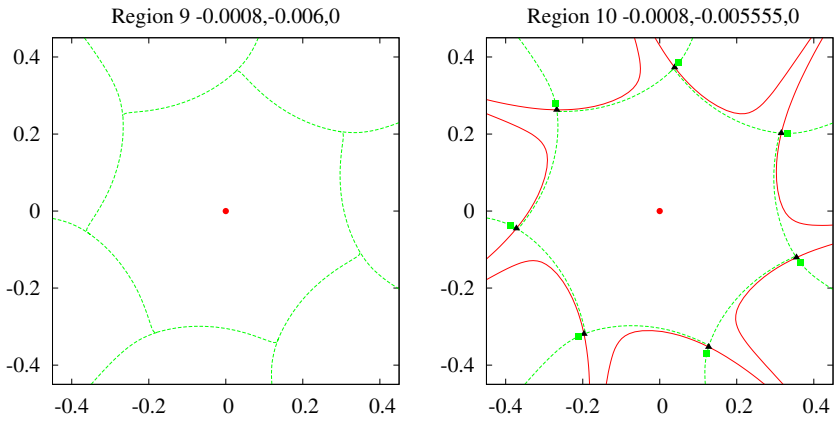

Figure 19. Continuation of figure 18, see figure 16 and the text in section 3.1 for details.

$\mathbb{Z}_7$-symmetric repelling equilibria, seven $\mathbb{Z}_7$-symmetric equilibria of saddle type and the stable manifolds of the latter. The transitions between the regions entail the following phenomena (see the corresponding phase portraits).

region 1 $\to$ 2: an attracting limit cycle is created;

region 2 $\to$ 7: the limit cycle enters a 1 : 7-resonance, where it consists of seven $\mathbb{Z}_7$-symmetric attracting equilibria, seven $\mathbb{Z}_7$-symmetric equilibria of saddle type and the unstable manifolds of the latter;

region 7 $\to$ 11: two sets of $\mathbb{Z}_7$-symmetric equilibria disappear through a saddle-node bifurcation taking place on the limit cycle. Due to the symmetry (20), regions 11 and 2 only differ by the the orientation of the spiralling around the origin.

Heteroclinic bifurcations. Along curve H_1^-, an equilibrium of saddle type develops a heteroclinic connection with another equilibrium of *the same* $\mathbb{Z}_7$-symmetric family, so a heteroclinic cycle [23, section 9.5] is formed (figure 20, top left panel). Heteroclinic cycles have various names in the literature, e.g. separatrix polygons [34], separatrix loops [35] and polycycles [20, 26]. We adopt the latter terminology. By Reyn's definition [34] polycycles are polygons, the corner points of which are saddle points, and the sides are formed by the separatrices connecting these saddle points.

In the generic case, more than one periodic orbit may arise by perturbing polycycles consisting of more than one equilibrium (see the above references). In the present $\mathbb{Z}_7$-symmetric case, polycycles formed by $\mathbb{Z}_7$-symmetric saddles are phenomenona of codimension 1 (if suitable non-degeneracy conditions are assumed). Indeed, a $\mathbb{Z}_7$-symmetric polycycle for $N_{\sigma,\tau}$ corresponds to a *homoclinic* saddle connection [19, section 6.1] for the vector field induced by $N_{\sigma,\tau}$ on the quotient space defined modulo the $\mathbb{Z}_7$-symmetry. For this reason, only one periodic orbit arises from the polycycle at H_1^- under parameter variation (assuming transversality and non-degeneracy). The stability of the periodic orbit depends on a quantity, which is a function of the eigenvalues of the equilibria in the polycycle [34]. We refer to this quantity as the saddle value (for analogy with the quotient case of saddle connections).

A degenerate polycycle (saddle value is zero) occurs at DH_1^-. This codimension 2 bifurcation point splits H_1^- into two branches (figure 16): in the upper (lower) branch, the

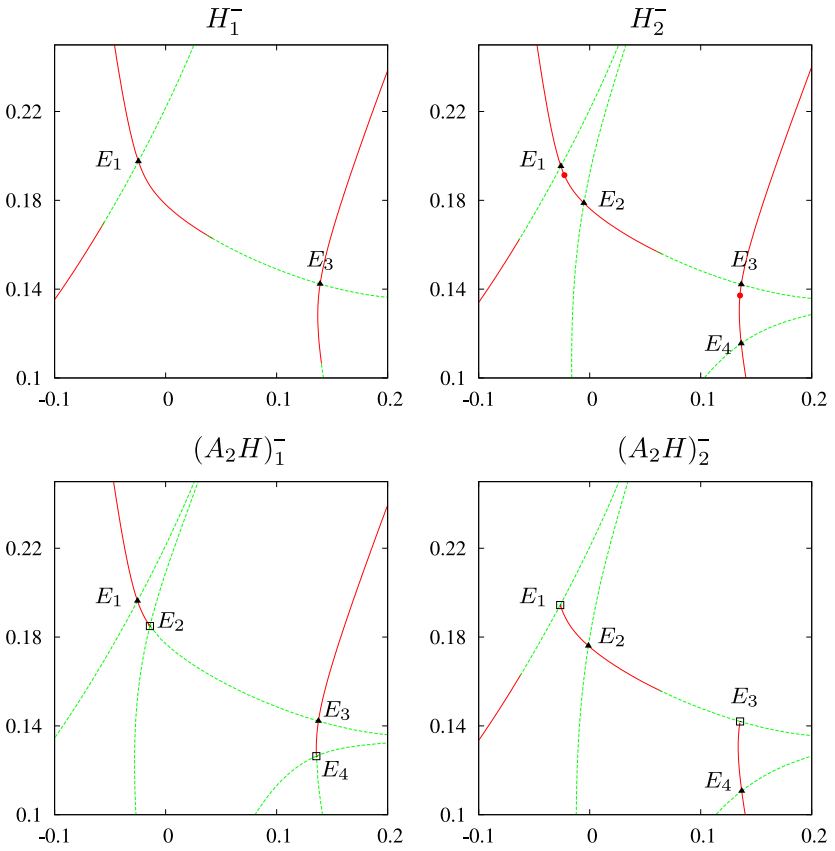

Figure 20. Top left: a heteroclinic connection forming a polycycle, occurring for parameters on curve H_1^-. Top right: a heteroclinic connection for parameters on curve H_2^- (no polycycle is formed here). Bottom left: degenerate polycycle occurring at point $(A_2H)_1^-$. The heteroclinic connection between $W^u(E_1)$ and $W^s(E_3)$ is interrupted by the occurrence of a saddle-node equilibrium E_2. Bottom right: degenerate heteroclinic connection occurring at point $(A_2H)_2^-$. A heteroclinic connection involves a family $E_2, E_4, \ldots, E_{14}$ of hyperbolic saddles and a family $E_1, E_3, \ldots, E_{13}$ of saddle-node equilibria, both families are $\mathbb{Z}_7$-symmetric. Connections are emphasized by only plotting part of $W^u(E_2)$ and $W^s(E_3)$.

saddle value is negative (positive). The following transitions appear near DH_1^-:

region $2 \to 3$ **(upper branch of** H_1^-**)**: the attracting periodic orbit (born at the Hopf curve *Ho*) disappears by merging into an attracting polycycle;
region $2 \to 4$ **(lower branch of** H_1^-**)**: from a repelling polycycle, a repelling periodic orbit is created, which also persists in region 5;
region $4 \to 3$ **(curve** L^-**)**: the repelling and attracting periodic orbits disappear at a saddle-node bifurcation; L^- is also the boundary between regions 5 and 6.

The heteroclinic bifurcations on curve H_2^- involve saddles E_1 and E_2 belonging to *two different* families of $\mathbb{Z}_7$-symmetric equilibria. For parameters on H_2^-, a branch of $W^u(E_1)$ is connected to a branch of $W^s(E_2)$, see figure 20, top right panel. However, the other branch of $W^u(E_1)$ ($W^s(E_2)$) converges to an attracting (repelling) node, so no polycycle is formed here.

A degenerate polycycle occurs at point $(A_2H)_1^-$. Here a family of $\mathbb{Z}_7$-symmetric saddle-node equilibria appears *along the connection*, see figure 20, bottom left panel. A family

$E_1, E_3, \ldots, E_{13}$ of $\mathbb{Z}_7$-symmetric hyperbolic saddles coexists with a family $E_2, E_4, \ldots, E_{14}$ of $\mathbb{Z}_7$-symmetric saddle-node equilibria. One branch of $W^u(E_1)$ and one branch of $W^s(E_3)$ converge to the two sides of the saddle-node equilibrium E_2; the latter only has a one-dimensional invariant manifold, which is $W^s(E_2)$. In other words, the polycycle is a centre manifold for the saddle-node bifurcation.

Another degenerate polycycle occurs at point $(A_2H)_2^-$. Here each of the saddle-node equilibria $E_1, E_3, \ldots, E_{13}$ has a heteroclinic connection (via its *one and only* one-dimensional invariant manifold, which is a stable manifold) with the unstable manifold of the hyperbolic saddles $E_2, E_4, \ldots, E_{14}$, see the bottom right panel of figure 20.

3.2. Tomogram with attached swallowtail

Figure 21 shows the extended bifurcation set corresponding to the two-dimensional tomogram of the resonance set in figure 15 (c), for $\tau = (-0.1, -0.0339)$. The phase portraits of several parameter regions are topologically equivalent to regions described in section 3.1 for $\tau = (-0.1, 0)$. The same labels are used, because this effectively identifies four-dimensional regions in (σ, τ)-parameter space. Phase portraits are deferred to appendix B and are only shown for the new regions as compared with section 3.1.

Many bifurcation curves and points occurring for $\tau = (-0.1, 0)$ (see section 3.1) are also present for $\tau = (-0.1, -0.0339)$. More precisely, the strata that reappear are the curves *Ho*, $L^{\pm}$ and H_1^+, the saddle-node curves corresponding to points of type A_2 strata in the resonance set and the point DH^+, where a polycycle with zero saddle value occurs. Additionally, the bifurcation diagram now involves many new phenomena. We start from two organizing centres HH_1 and HH_2, where codimension 2 polycycles occur.

Organizing centre HH_1. Figure 22 (left) shows the phase portrait of region 21: two families $E_1, E_3, \ldots, E_{13}$ and $E_2, E_4, \ldots, E_{14}$ of $\mathbb{Z}_7$-symmetric saddles coexist. A perturbation argument suggests that five types of heteroclinic connections may develop for nearby parameters. By $W_{i,j}$ we denote a connection occurs between $W^u(E_i)$ and $W^s(E_j)$: here (i, j) can be $(1, 3)$, $(1, 4)$, $(2, 3)$ and $(2, 4)$.

Remark 3.3.

(1) By the $\mathbb{Z}_7$-symmetry, connection $W_{1,2}$ also implies connection $W_{3,4}$.
(2) Connections $W_{1,3}$ and $W_{2,4}$ are codimension 1 polycycles, see section 3.1.

At the bifurcation point HH_1, all the above connections occur simultaneously, forming a star-like polycycle, which involves two distinct families of $\mathbb{Z}_7$-symmetric saddles. Modulo the $\mathbb{Z}_7$-symmetry (see section 3.1), each family would correspond to one saddle in the quotient space, yielding two in total, so we conclude that HH_1 is a codimension 2 bifurcation. All the five heteroclinic connections $W_{i,j}$ listed above are detected near HH_1. Denote as $H_{i,j}$ the parameter locus where connection $W_{i,j}$ occurs:

$H_{1,2}$ is the boundary between regions 21 and 7 and between 23 and 8;
$H_{1,3}$ is the boundary between 24 and 22;
$H_{1,4}$ is the boundary between 21 and 24;
$H_{2,3}$ is the boundary between regions 7 and 8 and between 26 and 23;
$H_{2,4}$ is the boundary between regions 18 and 19 and between 22 and 25.

The left panel in figure 23 displays a qualitative sketch of a neighbourhood of HH_1. The saddle value is always positive (negative) for the polycycles on bifurcation curve $H_{1,3}$ ($H_{2,4}$), corresponding to the creation of a repelling (attracting) periodic orbit. The 'corridor' between

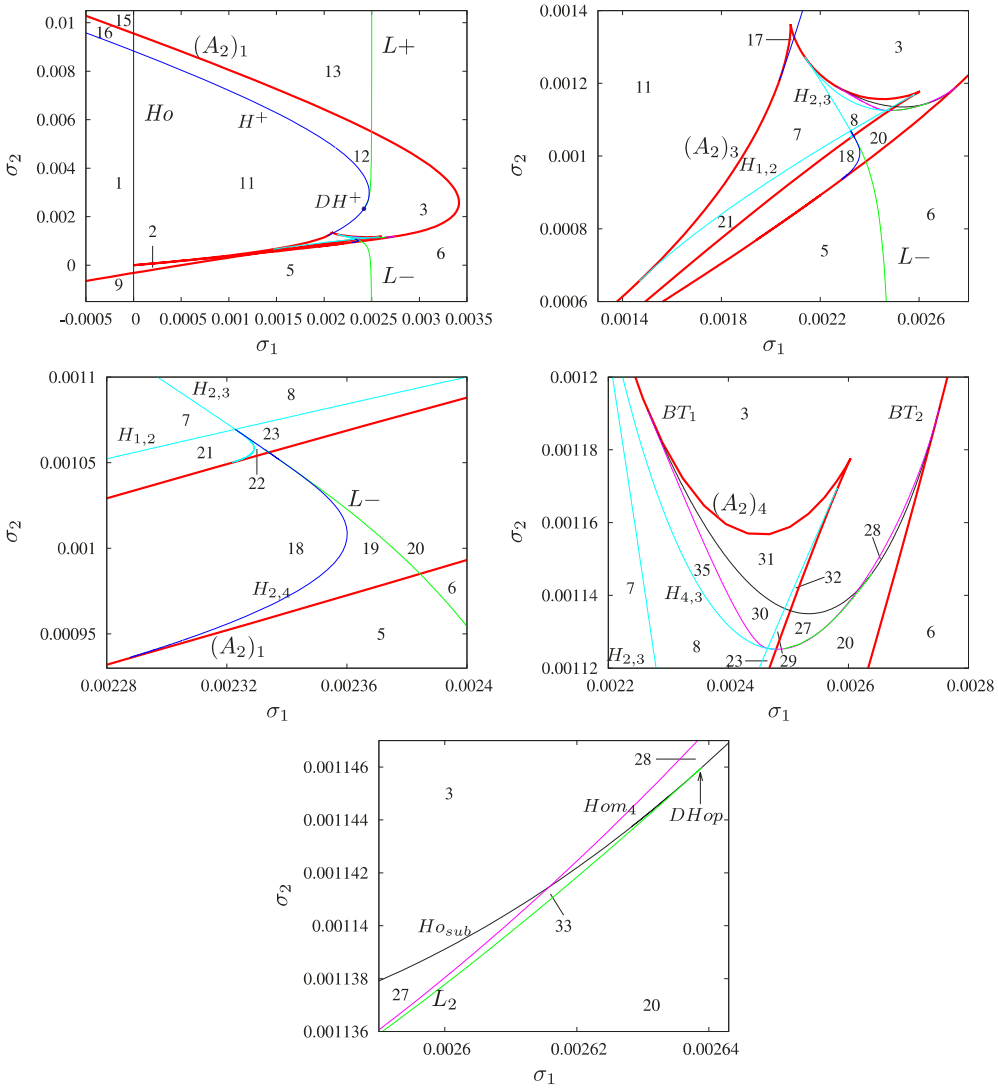

Figure 21. Bifurcation set of (19) for $\tau = (-0.1, -0.0339)$, with four subsequent magnifications in the σ-parameter plane near interesting regions. The curves of type A_2 are fatter to ease identification of the resonance set as illustrated in figure 15(*c*). See sections 3.1 and 3.2 for the meaning of the symbols. For phase portraits we refer to figures 17, 18 and 19 in section 3.1 and figures 25, 26 and 27 in appendix B.

$W^u(E_2)$ and $W^s(E_3)$ is rather narrow, see figure 22. Hence, the unstable manifolds $W^u(E_1)$ and $W^u(E_2)$ are very close to each other, as are the stable manifolds $W^s(E_3)$ and $W^s(E_4)$. As a result, the curves $H_{1,3}$ and $H_{1,4}$ are extremely close to each other in the parameter plane. What seems a single curve separating regions 21 and 22 in figure 21 is in fact a thin strip (region 24), bounded by $H_{1,4}$ at the left and by $H_{1,3}$ at the right, see the left panel of figure 23.

Actually, *infinitely many* other heteroclinic connections occur between $H_{1,4}$ and $H_{1,3}$. Indeed, consider again the left panel in figure 22 and denote the attracting nodes with $N_1, \ldots, N_7$. If $H_{1,4}$ is crossed transversally from left to right, then $W^u(E_1)$ crosses $W^s(E_4)$

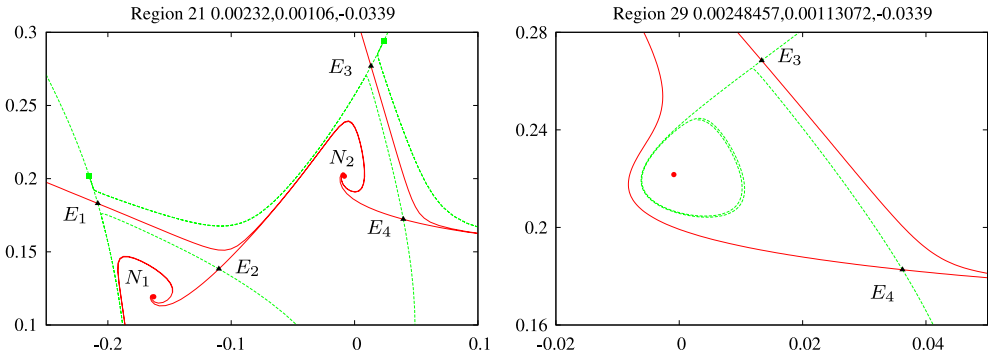

Figure 22. Left: magnification of phase portrait corresponding to region 21, illustrating that various types of heteroclinic connections can occur for nearby parameter values. Right: magnification of phase portrait corresponding to region 29, indicating that a heteroclinic connection can occur for nearby parameter values.

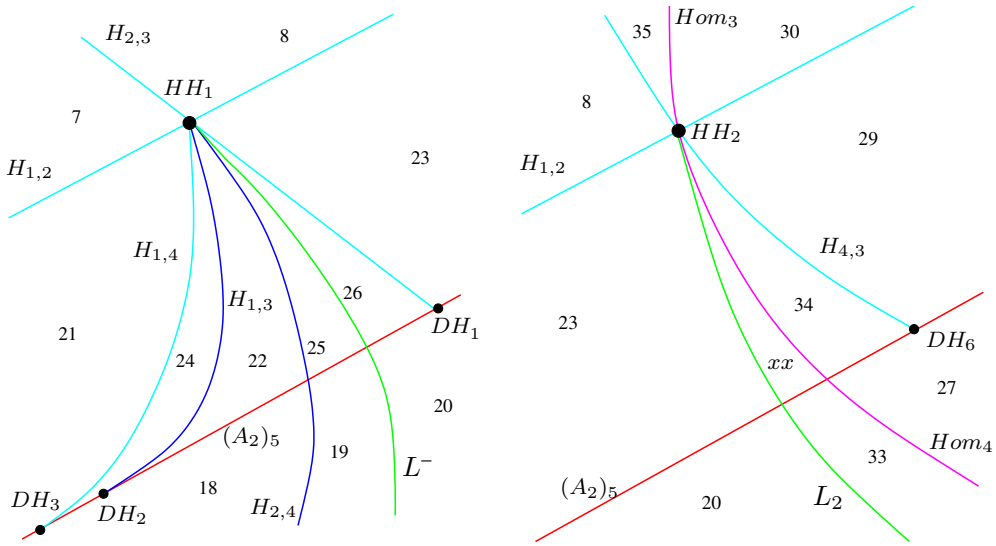

Figure 23. Magnifications of the bifurcation set in figure 21 near double heteroclinic points HH_1 (left panel) and HH_2 (right panel).

and is ultimately attracted by the node N_3 (not visible in the figure). For parameters near $H_{1,3}$, the unstable manifold $W^u(E_1)$ approaches E_3. However, before $W^u(E_1)$ can connect with $W^s(E_3)$, it must subsequently cross $W^s(E_6)$, $W^s(E_8)$ and so on. The bifurcation curves corresponding to these connections have not been computed.

Topological arguments suggested by the numerical results indicate that curves $H_{1,2}$ and $H_{2,3}$ have a transversal intersection across point HH_1, whereas $H_{1,3}$ and $H_{1,4}$ terminate at HH_1 where they are tangent to $H_{2,4}$. At the other endpoints, all these heteroclinic connection curves are tangent to the saddle-node curve A_2 corresponding to the resonance set in figure 15(c). One of these tangency points is close to a cusp, suggesting the presence of a codimension 3 cusp-heteroclinic connection in (σ, τ)-parameter space. Curve L^- becomes very close to $H_{2,4}$ near the point HH_1. Since the saddle value along $H_{2,4}$ is negative, curve L^- is not tangent to

$H_{2,4}$, and the only possibility is that it ends at HH_1 as well. It has been impossible to verify this with sufficient accuracy, due to the numerical limitation of double precision computations.

Closeness in parameter space corresponds to closeness of invariant manifolds in phase space. Hence, the two 'star-like' periodic orbits merging at L^- are always 'indistinguishably' close to each other in phase portraits for region 25, which is a very narrow subset of parameter space. The configuration of the latter phase portraits is topologically the same as the configuration for region 19, with the addition of seven repelling nodes and seven saddles created at a saddle-node curve. Similarly, the topology corresponding to region 26 is the same as the one corresponding to region 20 with the addition of seven nodes and seven saddles. The phase portrait of region 24 is difficult to interpret, because various invariant manifolds are very close to each other.

Organizing centre HH_2. The right panel in figure 22 shows the phase portrait for region 29, in which saddles are denoted consistently with the left panel. Repelling periodic orbits surround $\mathbb{Z}_7$-symmetric attracting equilibria. By a perturbation argument, a heteroclinic connection is expected between the 'downward' branch of $W^u(E_3)$ and the 'upward' branch of $W^u(E_4)$ for nearby parameter values. This leads to connection $W_{1,2}$ described above. After this has taken place, a saddle homoclinic connection of E_3 can occur. Another route starts again from region 29. For nearby parameter values the left branch of $W^u(E_4)$ can have a heteroclinic connection $W_{4,3}$ with the 'downward' branch of $W^s(E_3)$. After this has occurred, a homoclinic bifurcation of E_4 is possible. At bifurcation point HH_2 a codimension 2 polycycle is formed by the two simultaneous connections $W_{1,2}$ and $W_{4,3}$. The following bifurcation curves emerge from HH_2.

$H_{1,2}$ (also connected to HH_1) forms the boundary between regions 23 and 8, between regions 29 and 30 and between regions 32 and 31;
$H_{4,3}$ forms the boundary between regions 8 and 35 and between 34 and 29;
Hom_4 forms the boundary between regions 27 and 33 and between 28 and 3;
Hom_3 forms the boundary between regions 30 and 35.

The right panel in figure 23 presents a qualitative sketch of a neighbourhood of HH_2. Two periodic orbits are created at the saddle-node bifurcation of limit cycles curve L_2. The attracting orbit disappears at Hom_4, consistently with the saddle value of E_4 being negative [19, 23]. Since the saddle value of E_3 is positive along Hom_3, a repelling periodic orbit is created there, which is visible in the phase portraits of regions 27, 29, 30 and 33. It has proved impossible to draw the phase portrait of region xx, since the curves L_2 and Hom_4 are too close to each other to be resolved in double precision arithmetics. In phase space, this corresponds to an extreme closeness of the repelling periodic orbit to the homoclinic connection at Hom_4. Region 34 is also very narrow, due to the narrowness of the 'corridor' between the stable manifolds $W^s(E_3)$ and $W^s(E_4)$, see the right panel in figure 22.

The two branches Hom_3 and Hom_4 end at the two Bogdanov–Takens points BT_1, belonging to $(A_2)_1$ and BT_2 belonging to $(A_2)_2$, respectively. These points are also connected by a curve of Hopf bifurcations of equilibria. This Hopf curve is split into a supercritical and a subcritical branch (Ho_{sup} and Ho_{sub}, respectively) by a degenerate Hopf point $DHop$, where curve L_2 terminates, see the last panel of figure 21. The repelling periodic orbit born at the subcritical branch Ho_{sup} is the same as the one discussed above. The attracting periodic orbit born at the supercritical branch Ho_{sub} disappears at Hom_4. Additional degenerate Hopf points might be searched for by computing the first Lyapunov coefficient [23, section 3.5]. Presently we have not done so, only relying on phase portraits and topological reasoning.

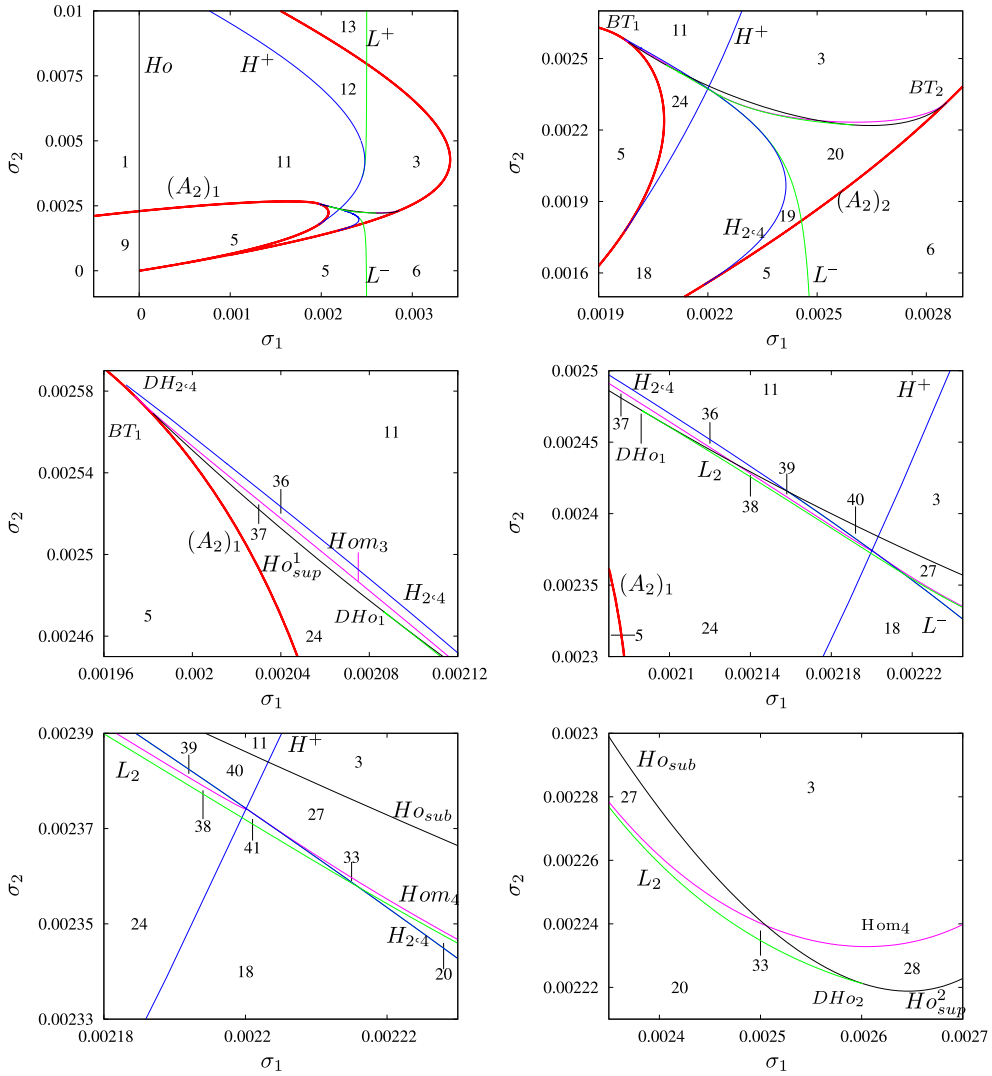

Figure 24. Bifurcation set of (19) for $\tau = (-0.1, -0.056)$, with five subsequent magnifications in the σ-parameter plane near interesting regions. The curves of type A_2 are plotted with fatter lines to ease identification of the resonance set as illustrated in figure 15(i). See sections 3.1, 3.2 and 3.3 for the meaning of the symbols. For phase portraits we refer to figures 17, 18 and 19 in section 3.1 and figures 25, 26, 27 and 28 in appendix B.

3.3. Tomogram without swallowtail

This section deals with the extension of the two-dimensional tomogram of the resonance set in figure 15(i), for $\tau = (-0.1, -0.056)$. In this case, all of the bifurcation curves occur for $\tau = (-0.1, -0.0339)$ as well, so the same notation as in the previous section has been retained. However, the relative positions of these curves is different and this yields several new regions in the parameter plane, see figure 24. Specifically, regions 36–41 are new, see appendix B for the phase portraits. We summarize the differences with the case described in the previous section.

- A new organizing centre HH_3 appears, where the two homoclinic bifurcation curves Hom_3 and Hom_4 intersect the curve $H_{2,4}$ of heteroclinic connections. The lower left panel in

figure 24 suggests that Hom_3 meets $H_{2,4}$ transversally and Hom_3 seems to intersect Hom_4 transversally as well. The saddle value along both branches $Hom_{3,4}$ is negative. Indeed, an attracting periodic orbit is seen in regions 39 and 33 to approach the saddle connection.

- Curve $H_{2,4}$ crosses curve H^+ past the intersection point HH_3, see figure 24, lower left panel. The saddle value along $H_{2,4}$ is always negative, implying that an attracting periodic orbit is formed and that curve L^- is not tangent to $H_{2,4}$. It has been impossible to compute L^- slightly above HH_3, since L^- is too close to $H_{2,4}$. Additional undetected regions must occur, such as a strip between 39 and 40, bounded from above by L^- and from below by $H_{2,4}$. Here a repelling periodic orbit coexists with an attracting periodic orbit and the former bounds an area in which the latter is contained, similar to the situation in region 19. Entering region 39 across $H_{2,4}$, the attracting periodic orbit disappears by merging with the heteroclinic cycle, whereas the repelling periodic orbit persists, see the phase portrait of region 39. A similar transition occurs between region 33 and 41.
- The saddle-node bifurcation of limit cycles curve L_2 is attached to degenerate Hopf points DHo_1 and DHo_2. Therefore, the Hopf curve is split into the pair of supercritical branches Ho^1_{sup} and Ho^2_{sup} and the subcritical branch Ho_{sub}, bounded between DHo_1 and DHo_2.

3.4. Expectations for mildly degenerate universal family of diffeomorphisms

We now discuss the implications for the universal family of planar diffeomorphisms, $P_{\sigma,\tau}$ given in (4), of the bifurcation diagram of the planar vector field family $N_{\sigma,\tau}$, given in (19), described in the previous sections. We recall that these families are related by

$$P_{\sigma,\tau}(z) = \Omega_{p/q} \circ N^1_{\sigma,\tau}(z) + O(|\sigma|^2, |\tau|^2, |z|^q).$$

First of all, local phenomena are persistent under $O(|\sigma|^2, |\tau|^2, |z|^q)$ perturbations. This holds for all hyperbolic equilibria, their linear type and corresponding local bifurcation strata. So, e.g., a hyperbolic equilibrium of $N_{\sigma,\tau}$ corresponds to a hyperbolic periodic point of $P_{\sigma,\tau}$ and a saddle-node bifurcation of equilibria for $N_{\sigma,\tau}$ corresponds to a saddle-node bifurcation of periodic orbits for $P_{\sigma,\tau}$. A list of features which are expected to persist for $P_{\sigma,\tau}$ with trivial (or, in any case, not too involved) modifications is summarized in the top part of table 3. The persistence properties of more degenerate local bifurcations of $N_{\sigma,\tau}$ and $P_{\sigma,\tau}$, which are excluded from table 3 are easily deduced from the given information.

Heteroclinic and homoclinic connections of $N_{\sigma,\tau}$ do not persist generically for $P_{\sigma,\tau}$. The expectation is that they are generically replaced by heteroclinic and homoclinic tangles, respectively, which are transversal heteroclinic or homoclinic intersections of invariant manifolds [1, 19, 23, 22, 37]. Such transversal intersections are persistent under small perturbations: therefore, curves such as H^-_1 in figure 16 'split' into open domains within (σ, τ)-parameter space. Chaotic dynamics, due to the presence of horseshoes, may be expected in such domains [11, 23] and chaotic attractors may occur near the expected tangencies between invariant manifolds, which is a codimension 1 phenomenon [29].

4. Conclusion and future work

This paper presents a study of the resonance set of a universal 4-parameter HNS family of planar diffeomorphisms, providing a Whitney stratification and thereby yielding a better understanding of the corresponding geometry. Our approach consists of analysing the Whitney stratification by explicitly determining the incidence relations between the strata and taking appropriate two- and three-dimensional tomograms. This approach serves as a paradigm for the investigation of other complicated higher dimensional (bifurcation) sets.

Table 3. Relations between the dynamics of the universal family of the mildly degenerate case $P_{\sigma,\tau}$ and its Takens normal form vector field approximation $N_{\sigma,\tau}$. Here $\Omega_{p/q}$ is a rotation over $2\pi p/q$ around the origin. Combinations of the listed bifurcations also occur, see sections 3.1, 3.2 and 3.3. Degenerate HNS bifurcations in families of maps are studied in [13].

$P_{\sigma,\tau}$	$N_{\sigma,\tau}$
Fixed point	Equilibrium
q-periodic orbit	q different equilibria invariant under $\Omega_{p/q}$
(Degenerate) HNS bifurcation	(Degenerate) Hopf bifurcation
Saddle-node (A_2) bif. of q-periodic orbit	Saddle-node (A_2) bif. of q different equilibria
Cusp (A_3) bifurcation of q-periodic orbit	Cusp (A_2) bif. of q different equilibria
Homoclinic tangle	Homoclinic connection
Heteroclinic tangle	Heteroclinic connection

We also show that the resonance set, up to a small diffeomorphic distortion, forms only a small part of a more complicated bifurcation set, which is obtained using a Takens normal form vector field approximation of the family of diffeomorphisms. The two-dimensional tomograms of parameter space investigated for this family of vector fields demonstrate a rich variety of bifurcations including (degenerate) Hopf, homoclinic, heteroclinic and Bogdanov–Takens bifurcations. A more complete study of the bifurcation set of both the mildly degenerate universal family and the corresponding vector field approximation remains future work.

Moreover, we plan to extend our work on, e.g., recognition problems [7] and visualization of bifurcation and resonance sets to families of flows near resonance. The development of effective methods requires a combination of symbolic and numerical methods.

Acknowledgments

RV is indebted to the University of Groningen for kind hospitality and gratefully acknowledges support by the Willis Research Network (www.willisresearchnetwork.com).

Appendix A. Computations

In this appendix we present proofs of the theorems given in section 2.2. We start with a parametrization of $D(p_{\varepsilon,\sigma,\tau})$ with $p_{\varepsilon,\sigma,\tau}$ as in (15), then we prove theorem 2.1. Finally, we prove theorem 2.2 by first providing parametrizations of the codimension 3 strata in $D(p_{\varepsilon,\sigma,\tau})$ in appendix A.3 and then check the versality conditions for these strata in appendix A.4.

Appendix A.1. Parametrization of $D(p_{\varepsilon,\sigma,\tau})$

In theorem A.1 we give a parametrization of $D(p_{\varepsilon,\sigma,\tau})$. As a consequence the Hausdorff distance between $D(p_{\varepsilon,\sigma,\tau})$ and $D(p_{0,\sigma,\tau})$ is easily computed.

Theorem A.1 (Parametrization of $D(p_{\varepsilon,\sigma,\tau})$). *The map $\Gamma^{\varepsilon,\pm} : \mathbb{R}_+ \times \mathbb{R}^2 \to \mathbb{R}^4$, which gives a parametrization of $D(p_\varepsilon)$, is given by*

$$\Gamma^{\varepsilon,\pm}(u,\tau) = (\sigma_{1_0}(u,\tau) + M^{\varepsilon,\pm}(u,\tau), \sigma_{2_0}(u,\tau) + N^{\varepsilon,\pm}(u,\tau), \tau_1, \tau_2), \qquad (21)$$

with

$$\sigma_{1_0}(u,\tau) = -u(\tau_1 + u),$$

$$\sigma_{2_0}(u,\tau) = -\tau_2 u,$$

$$M^{\varepsilon,\pm}(u,\tau) = \frac{1}{2D(u,\tau)}((q-2)\varepsilon^{q-6}u^{q-3}(\tau_1+2u)$$
$$\pm\varepsilon^{(q-6)/2}\tau_2 u^{(q-2)/2}\sqrt{4D(u,\tau)-(q-2)^2\varepsilon^{q-6}u^{q-4}}),$$
$$N^{\varepsilon,\pm}(u,\tau) = \frac{1}{2D(u,\tau)}((q-2)\varepsilon^{q-6}\tau_2 u^{q-3}$$
$$\mp\varepsilon^{(q-6)/2}(\tau_1+2u)u^{(q-2)/2}\sqrt{4D(u,\tau)-(q-2)^2\varepsilon^{q-6}u^{q-4}}),$$

where

$$D(u,\tau) = (\tau_1+2u)^2+\tau_2^2. \tag{22}$$

Proof. First of all we rewrite $p_{\varepsilon,\sigma,\tau}$ given in (15) by putting $\tau = \tau_1 + \mathrm{i}\tau_2$ and $\sigma = \sigma_1 + \mathrm{i}\sigma_2$, resulting in

$$p_{\varepsilon,\sigma,\tau}(u;\sigma,\tau) = -\varepsilon^{q-6}u^{q-2}+u^4+2\tau_1u^3+(|\tau|^2+2\sigma_1)u^2+2(\tau_1\sigma_1+\tau_2\sigma_2)u+|\sigma|^2.$$

Secondly, we use that $(\tau_1, \tau_2, \sigma_{1_0}(u,\tau), \sigma_{2_0}(u,\tau))$ parametrizes $D(p_{0,\sigma,\tau})$, which immediately follows from $p_{0,\sigma,\tau}(u) = 0$ and $(\partial p_{0,\sigma,\tau}/\partial u)(u) = 0$. A parametrization of $D(p_{\varepsilon,\sigma,\tau})$ is then obtained as a perturbation by putting

$$(\sigma_1,\sigma_2) = (\sigma_{1_0}(u,\tau)+M, \sigma_{2_0}(u,\tau)+N).$$

Plugging this into the equations that define $D(p_{\varepsilon,\sigma,\tau})$, that is $p_{\varepsilon,\sigma,\tau}(u) = 0$ and $(\partial p_{\varepsilon,\sigma,\tau}/\partial u)(u) = 0$, yields

$$\begin{aligned} &M^2+N^2-\varepsilon^{q-6}u^{q-4} = 0,\\ &2\tau_1M+2\tau_2N+4Mu-(q-2)\varepsilon^{q-6}u^{q-3} = 0 \end{aligned} \tag{23}$$

These equations have the 2 real solutions $M^{\varepsilon,\pm}$ and $N^{\varepsilon,\pm}$ as defined in theorem A.1 for M and N, respectively. □

The latter proof allows us to show that the Hausdorff distance between $D(p_{\varepsilon,\sigma,\tau})$ and $D(p_{0,\sigma,\tau})$ is $O(\varepsilon^{(q-6)/2})$. The first step is restricting to bounded sets. Therefore, we assume that $u \leqslant U$ and $|\tau| \leqslant T$, since then $\Gamma^{\varepsilon,\pm}$ parametrizes a bounded subset of $D(p_{\varepsilon,\sigma,\tau})$ near $(\sigma,\tau) = (0,0)$ for each ε. In this case, an upper bound for the Hausdorff distance between $D(p_{\varepsilon,\sigma,\tau})$ and $D(p_{0,\sigma,\tau})$ is determined as follows,

$$d_H(D(p_{\varepsilon,\sigma,\tau}), D(p_{0,\sigma,\tau}))^2 \leqslant \sup_{u\leqslant U,|\tau|\leqslant T}\{d(\Gamma^{\varepsilon,\pm}(u,\tau), \Gamma^{0,\pm}(u,\tau))^2\}$$
$$= \sup_{u\leqslant U,|\tau|\leqslant T}\{M^{\varepsilon,\pm}(u,\tau)^2+N^{\varepsilon,\pm}(u,\tau)^2\}.$$

Since $M^{\varepsilon,\pm}$ and $N^{\varepsilon,\pm}$ are solutions to (23), this results in $d_H(D(p_{\varepsilon,\sigma,\tau}), D(p_{0,\sigma,\tau})) \leqslant \varepsilon^{(q-6)/2}U^{(q-4)/2}$.

A.2. Proof of theorem 2.1

Here theorem 2.1 is proven by giving an extended version.

Theorem A.2 (Whitney stratification of $D(p_{0,\sigma,\tau})$). *The discriminant set $D(p_{0,\sigma,\tau})$ is given by*

$$D(p_{0,\sigma,\tau}) = \{(\sigma_1,\sigma_2,\tau_1,\tau_2)\in\mathbb{R}^4 \mid \sigma_1 = -u(\tau_1+u), \sigma_2 = -\tau_2 u, u\in\mathbb{R}_+\}, \tag{24}$$

which is the closure of the stratum of type A_2. This set is diffeomorphic to the product of the real line and a subset of the Whitney umbrella W defined in (9).

The set $D(p_{0,\sigma,\tau})$ has a codimension 2 stratum of type A_2^2 given by the following set,

$$A_2^2 = \{(\sigma_1, \sigma_2, \tau_1, \tau_2) \in \mathbb{R}^4 \mid \tau_1 \leqslant 0, \tau_2 = 0, 0 \leqslant \sigma_1 \leqslant -\tau_1^2/4, \sigma_2 = 0\}.$$

The codimension 2 stratum of type ∂A_2 is given by

$$\partial A_2 = \{(\sigma_1, \sigma_2, \tau_1, \tau_2) \in \mathbb{R}^4 \mid \sigma_1 = 0, \sigma_2 = 0\}. \tag{25}$$

For all fixed $\tau_1 \leqslant 0$ the stratum of type A_2^2 is attached to the codimension 3 strata of type ∂A_2^2 and P given by

$$\partial A_2^2 = \{(\sigma_1, \sigma_2, \tau_1, \tau_2) \in \mathbb{R}^4 \mid \tau_1 \leqslant 0, \tau_2 = 0, \sigma_1 = 0, \sigma_2 = 0\}$$

and

$$P = \left\{(\sigma_1, \sigma_2, \tau_1, \tau_2) \in \mathbb{R}^4 \mid \tau_1 \leqslant 0, \tau_2 = 0, \sigma_1 = -\frac{\tau_1^2}{4}, \sigma_2 = 0\right\}.$$

This implies that the strata of type ∂A_2^2 and P meet in $(\sigma_1, \sigma_2, \tau_1, \tau_2) = (0, 0, 0, 0)$, the central singularity.

Proof. The parametrization of $D(p_{0,\sigma,\tau})$, by definition the closure of all strata of type A_2, follows from theorem A.1. This parametrization leads to the implicit representation of $D(p_{0,\sigma,\tau})$ given by

$$\{(\sigma_1, \sigma_2, \tau_1, \tau_2) \in \mathbb{R}^4 \mid \tau_2^2\sigma_1 - \tau_1\tau_2\sigma_2 + \sigma_2^2 = 0, \quad \operatorname{sign}(\sigma_2) = -\operatorname{sign}(\tau_2)\},$$

which is diffeomorphic to the product of the real line and a subset of the Whitney umbrella W given in (9). Moreover, the condition $\operatorname{sign}(\sigma_2) = -\operatorname{sign}(\tau_2)$ implies that the stratum of type A_2 is attached to a stratum of type ∂A_2 given in (25).

To determine a parametrization of the stratum of type A_2^2 and the codimension 3 strata it is attached to, we rewrite the implicit equation giving $D(p_{0,\sigma,\tau})$ for $\tau_2 \neq 0$ to

$$\sigma_1 = -\frac{\sigma_2^2}{\tau_2^2} + \frac{\tau_1\sigma_2}{\tau_2} = -\left(\frac{\sigma_2}{\tau_2} + \frac{\tau_1}{2}\right)^2 + \frac{\tau_1^2}{4}, \tag{26}$$

which gives a parabola in the σ-plane, if τ_1 and τ_2 are considered as parameters. This parabola gets narrower as τ_2 tends to 0, so comparing with the Whitney umbrella we conclude that for $\tau_2 = 0$ there are self-intersection points in $D(p_{0,\sigma,\tau})$. The parametrization in (24) yields that σ_1 assumes all values of the set $[0, \tau_1^2/4)$ twice for $u \in [0, -\tau_1/2) \cup (-\tau_1/2, -\tau_1]$, giving intersection points if $\tau_2 = 0$ (this implies $\sigma_2 = 0$ by (24)). These points only occur for $\tau_1 < 0$, because $u > 0$, so the self-intersection points (A_2^2) are given by (25). □

A.3. Parametrizations of codimension 3 strata in $D(p_{\varepsilon,\sigma,\tau})$

Here we prove the incidence relations of the Whitney stratification of $D(p_{\varepsilon,\sigma,\tau})$ presented in theorem 2.2. Therefore, we show that independent of q, there are only 3 pairs of codimension 3 strata attached to $(\sigma, \tau) = (0, 0)$, see theorem A.3. These strata determine all incidence relations, which are deduced from two- or three-dimensional tomograms of $D(p_{1,\sigma,\tau})$, see section 2.2.

Moreover, the Hausdorff distances between strata given in theorem 2.2 follow immediately from the parametrizations given in theorem A.3. We note that this theorem also contains a parametrization of $T^{\pm}$ to show that they meet in $(\sigma, \tau) = (0, 0)$, see figure 15.

Theorem A.3. *There are 3 pairs of codimension 3 strata attached to* $(\sigma, \tau) = (0, 0)$. *The strata* $(A_4)_1^{\pm}$ *are parametrized by* $\Gamma_1^{\varepsilon,\pm} : \mathbb{R}_+ \to \mathbb{R}^4$ *given by*

$$\Gamma_1^{\varepsilon,\pm}(u) = \left\{ u^2 + O(\varepsilon^{q-6}), \mp\frac{(q-2)\varepsilon^{(q-6)/2}u^{(q-2)/2}}{2} + O(\varepsilon^{q-6}), \right.$$
$$\left. -2u + O(\varepsilon^{q-6}), \pm\frac{(q-2)\varepsilon^{(q-6)/2}u^{(q-4)/2}}{2} + O(\varepsilon^{q-6}) \right\}. \tag{27}$$

The curves $T^{\pm}$ *are parametrized by* $\Gamma_2^{\varepsilon,\pm} : \mathbb{R}_+ \to \mathbb{R}^4$ *given by*

$$\Gamma_2^{\varepsilon,\pm} = \left\{ \frac{1}{a}u^2 + O(\varepsilon^{q-6}), \mp b\varepsilon^{(q-6)/2}u^{(q-2)/2} + O(\varepsilon^{q-6}), \right.$$
$$\left. -\frac{1}{a}u + O(\varepsilon^{q-6}), \pm b\varepsilon^{(q-6)/2}u^{(q-4)/2} + O(\varepsilon^{q-6}) \right\}, \tag{28}$$

where $b = (a^{(q-2)/2} + (1-a)^{(q-2)/2})/(a^{(q-4)/2}(1-2a))$ *and* a *is a solution of*

$$d\frac{(1-a)^{(q-2)/2} + a^{(q-2)/2}}{2a-1}{da} = 0. \tag{29}$$

For $q = 7$ *this gives* $a = 1/2 - \sqrt{5}/6$.
The strata $(R_q A_2)^{\pm}$ *are parametrized by* $\Gamma_3^{\varepsilon,\pm} : \mathbb{R}_+ \to \mathbb{R}^4$ *given by*

$$\Gamma_3^{\varepsilon,\pm}(u) = \{0, 0, -u + O(\varepsilon^{q-6}), \pm\varepsilon^{(q-6)/2}u^{(q-4)/2} + O(\varepsilon^{q-6})\}. \tag{30}$$

Finally, the strata $(A_4)_2^{\pm}$ *are parametrized by* $\Gamma_4^{\varepsilon,\pm} : \mathbb{R}_+ \to \mathbb{R}^4$ *given by*

$$\Gamma_4^{\varepsilon,\pm}(u) = \{u^2 + O(\varepsilon^{q-6}), \mp\sqrt{2}\varepsilon^{(q-6)/4}u^{(q+2)/4} + O(\varepsilon^{(q-6)/2}),$$
$$-2u + O(\varepsilon^{(q-6)}), \pm\sqrt{2}\varepsilon^{(q-6)/4}u^{(q-2)/4} + O(\varepsilon^{(q-6)/2})\}. \tag{31}$$

For proving theorem A.3 we use the following lemma containing parametrizations of R_q and of strata of type A_3.

Lemma A.1. *The entire* τ*-plane except for* $\tau = 0$ *consists of points of type* R_q.

Furthermore, a parametrization of strata of type A_3*, assuming that* $\tau_1 + 2u = O(\varepsilon^{q-6})$ *and that* τ_2 *is of lower order than* $O(\varepsilon^{(q-6)/2})$*, is given by* $\Gamma^{\varepsilon,\pm} \circ t_1^{\varepsilon,\pm}$*, where* $t_1^{\varepsilon,\pm} : \mathbb{R}_+ \times \mathbb{R} \to \mathbb{R}_+ \times \mathbb{R}^2$ *is given by*

$$t_1^{\varepsilon,\pm} : (u, \tau_1) \mapsto (u, \tau_1, \tau_2) = (u, \tau_1, \pm\sqrt{2}\varepsilon^{(q-6)/4}u^{(q-2)/4} + O(\varepsilon^{(q-6)/2})).$$

If $\tau_2 + 2u = O(\varepsilon^{q-6})$ *and* $\tau_2 = O(\varepsilon^{(q-6)/2})$*, then a local parametrization of* A_3 *points is given by* $\Gamma^{\varepsilon,\pm} \circ t_2^{\varepsilon,\pm}$*, where* $t_2^{\varepsilon,\pm} : \mathbb{R}_+ \times \mathbb{R} \to \mathbb{R}_+ \times \mathbb{R}^2$ *is given by*

$$t_2^{\varepsilon,\pm} : (u, \tau_1) \mapsto (u, \tau_1, \tau_2) = \left(u, \tau_1, \pm\frac{q-2}{2}\varepsilon^{(q-6)/2}u^{(q-4)/2} + O(\varepsilon^{q-6})\right).$$

Proof. The statement that the τ-plane apart from $\tau = 0$ is a stratum of type R_q follows immediately from the recognition conditions for strata of type R_q given in [7]. This result is obtained by returning to the family $P_{\sigma,\tau}$ given in (6), which gives rise to $p_{\varepsilon,\sigma,\tau}$. It follows that for $\sigma = 0$ and $\tau \neq 0$ the corresponding generalized Lyapunov–Schmidt reduction is $\mathbb{Z}_q$-equivariant contact-equivalent to the Lyapunov–Schmidt reduced central singularity of P_σ as in (1). Moreover, the generalized Lyapunov–Schmidt reduction of $P_{\sigma,\tau}$ is a versal unfolding of these singularities.

Now we turn to determining parametrizations for strata of type A_3. For this we use that these points are on the discriminant set D_ε and also satisfy $(\partial^2 p_{\varepsilon,\sigma,\tau}/\partial u^2)(u) = 0$, yielding

$$\tau_2^2 = \tfrac{1}{2}(q^2 - 5q + 6)\varepsilon^{q-6}u^{q-4} - 6u^2 - 6\tau_1 u - \tau_1^2 - 2\sigma_1. \tag{32}$$

Next we substitute the σ_1-component of $\Gamma^{\varepsilon,\pm}$, from now on denoted by $(\Gamma^{\varepsilon,\pm})_{\sigma_1}$, in (32), which yields

$$\tau_2^2 = -6u^2 - 6\tau_1 u - \tau_1^2 + 2u(\tau_1 + u) \pm 2\frac{\varepsilon^{(q-6)/2}\tau_2 u^{(q-2)/2}}{\sqrt{\tau_2^2 + (\tau_1 + 2u)^2}} + O(\varepsilon^{q-6}),$$

assuming that τ_2 is of lower order in ε than $\tau_1 + 2u$. More specifically, a non-trivial solution for τ_2 is obtained if $2u + \tau_1 = O(\varepsilon^{q-6})$ and τ_2 is of lower order than $O(\varepsilon^{q-6})$. Indeed, in that case the latter equation reduces to

$$\tau_2 = \pm\sqrt{2}\varepsilon^{(q-6)/4}u^{(q-2)/4} + O(\varepsilon^{(q-6)/2}).$$

It turns out that two other real solutions of (32) can be obtained if $\tau_2 = O(\varepsilon^{(q-6)/2})$ and $\tau_1 + 2u = O(\varepsilon^{q-6})$. In this case, we have that $D(u, \tau)$ as defined in (22) is of order $O(\varepsilon^{q-6})$, so we need to substitute $(\Gamma^{\varepsilon,\pm})_{\sigma_1}$ entirely in (32). Keeping only the terms that are of lowest order in ε yields

$$0 = 4D(u, \tau) - (q-2)^2\varepsilon^{q-6}u^{q-4} + O(\varepsilon^{2(q-6)}) \tag{33}$$

which has the following real solutions,

$$\tau_2 = \pm\frac{q-2}{2}\varepsilon^{(q-6)/2}u^{(q-4)/2} + O(\varepsilon^{q-6}).$$

We note that if τ_2 is assumed to be of higher order than $O(\varepsilon^{(q-6)/2})$, a contradiction with $\tau_1 + 2u = O(\varepsilon^{q-6})$ easily follows. □

Finally, we are in the position to prove theorem A.3.

Proof. We start with computing the parametrizations of $(A_4)_1^{\pm}$ and $(A_4)_2^{\pm}$. These points are attached to strata of type A_3 and, additionally, satisfy $(\partial^3 p_{\varepsilon,\sigma,\tau}/\partial u^3)(u) = 0$, yielding

$$\tau_1 = -2u + \tfrac{1}{12}(q-4)(q-3)(q-2)\varepsilon^{q-6}u^{q-5}, \tag{34}$$

this means $\tau_1 + 2u = O(\varepsilon^{q-6})$. Consequently, the results of lemma A.1 can be used. Substituting the latter equation in $t_1^{\varepsilon,\pm}$ and $t_2^{\varepsilon,\pm}$ yields that the τ_2 component of the codimension 3 strata satisfies either

$$\tau_2 = \pm\sqrt{2}\varepsilon^{(q-6)/4}u^{(q-2)/4} + O(\varepsilon^{(q-6)/2})$$

or

$$\tau_2 = \pm\frac{(q-2)\varepsilon^{(q-6)/2}u^{(q-4)/2}}{2} + O(\varepsilon^{q-6}).$$

Substituting the latter equations and $\tau_1 = -2u + O(\varepsilon^{q-6})$ in $\Gamma^{\varepsilon,\pm}$ gives approximate parametrizations of $(A_4)_2^{\pm}$ and $(A_4)_1^{\pm}$, respectively.

Here we determine a parametrization of the curves $(R_q A_2)^{\pm}$. By lemma A.1 parameter values on R_q satisfy $\sigma = 0$, yielding

$$p_{\varepsilon,0,\tau}(u) = u^2(-\varepsilon^{q-6}u^{q-4} + u^2 + 2\tau_1 u + |\tau|^2).$$

This is also a point of type A_2 if

$$\frac{p_{\varepsilon,0,\tau}(u)}{u^2} = 0 \qquad \text{and} \qquad \frac{\partial p_{\varepsilon,0,\tau}/u^2}{\partial u}(u) = 0,$$

which is easily solved by

$$\tau_1 = -u + \frac{q-4}{2}\varepsilon^{q-6}u^{q-5}$$

and

$$\tau_2 = \pm\varepsilon^{(q-6)/2}u^{(q-4)/2} + O(\varepsilon^{q-6}).$$

Substituting these in $\Gamma^{\varepsilon,\pm}$ yields the parametrization of $(R_q A_2)^{\pm}$.

Next we obtain the parametrizations for $T^{\pm}$. We recall that T^+ and T^- are determined by the points where a two-dimensional tomogram with τ fixed is not transversal to the self-intersection strata $(A_2^2)_1^+$ and $(A_2^2)_1^-$, respectively. Hence, we start with a parametrization of $(A_2^2)_1^{\pm}$ taking into account that the pair $T^{\pm}$ belongs to the subset of $D(p_{\varepsilon,\sigma,\tau})$ parametrized by $\Gamma^{\varepsilon,-}$, see (21) and figure 15. Therefore, we determine when $\Gamma^{\varepsilon,-}(u,\tau)$ has 2 different values of u denoted by u_1 and u_2 such that for τ fixed $(\Gamma^{\varepsilon,-})_{\sigma_1}(u_1,\tau) = (\Gamma^{\varepsilon,-})_{\sigma_1}(u_2,\tau)$ and $(\Gamma^{\varepsilon,-})_{\sigma_2}(u_1,\tau) = (\Gamma^{\varepsilon,-})_{\sigma_2}(u_2,\tau)$. Clearly, this gives a self-intersection point for $u_1 \neq u_2$. First we consider $(\Gamma^{\varepsilon,-})_{\sigma_1}$ given by

$$(\Gamma^{\varepsilon,\pm})_{\sigma_1}(u,\tau) = -u(\tau_1 + u) + O(\varepsilon^{q-6}).$$

It follows that for $u_1 = -a\tau_1 + O(\varepsilon^{q-6})$ and $u_2 = -(1-a)\tau_1 + O(\varepsilon^{q-6})$ with $0 < a < 1/2$ this component has the same value. For $(\Gamma^{\varepsilon,-})_{\sigma_2}$ we obtain

$$-\tau_2 u_1 + \varepsilon^{(q-6)/2}u_1^{(q-2)/2} = -\tau_2 u_2 + \varepsilon^{(q-6)/2}u_2^{(q-2)/2} + O(\varepsilon^{q-6}), \tag{35}$$

assuming that $\tau_1 + 2u_i = O(\varepsilon^0)$ for $i = 1, 2$, which is the case for points that are not close to $(A_4)_1^{\pm}$ and $(A_4)_2^{\pm}$. Figure 12 shows that to solve this equation, we only need a parametrization of self-intersection points for τ values between the projections of $(A_4)_1^{\pm}$ and $(R_q A_2)^{\pm}$ implying the form

$$\tau_2 = \pm b\varepsilon^{(q-6)/2}u^{(q-4)/2} + O(\varepsilon^{q-6}),$$

where b is some real number. Substituting the latter equation, $u_1 = -a\tau_1 + O(\varepsilon^{q-6})$ and $u_2 = -(1-a)\tau_1 + O(\varepsilon^{q-6})$ in (35) yields

$$b = \pm\frac{a^{(q-2)/2} + (1-a)^{(q-2)/2}}{a^{(q-4)/2}(2a-1)}. \tag{36}$$

This means the self-intersection points near $(R_q A_2)^{\pm}$ are parametrized by $\Gamma^{\varepsilon,-} \circ t_3^{\varepsilon,\pm}$, where $t_3^{\varepsilon,\pm} : \mathbb{R}_+ \times \mathbb{R} \to \mathbb{R}_+ \times \mathbb{R}^2$ is given by

$$t_3^{\varepsilon,\pm} : (u,\tau_1) \mapsto (u,\tau_1,\tau_2) = (u,\tau_1,\pm b\varepsilon^{(q-6)/2}u^{(q-4)/2} + O(\varepsilon^{q-6})),$$

with b as given in (36). It remains to determine where these points are not transversal to a tomogram with τ fixed, i.e. for which u the self-intersection points touch a two-dimensional tomogram with especially τ_2 fixed. Thus, we need to solve

$$\frac{\partial (t_3^{\pm})_{\tau_2}}{\partial u}(u,\tau_1,\tau_2) = 0.$$

Using that $u = u_1 = -a\tau_1 + O(\varepsilon^{q-6})$, this leads to (29), which is difficult to solve for general q; however, with the help of `Mathematica` [41] solutions can be obtained, see theorem A.3. We remark that these solutions tend to $1/2$, i.e. $a \to 1/2$, for $q \to \infty$, meaning that for large q the condition $\tau_1 + 2u_i = O(\varepsilon^0)$ for $i = 1, 2$ is broken. Consequently, for large q a different approach from the one above is required to determine parametrizations for $T^{\pm}$. Since $T^{\pm}$ is not part of the Whitney stratification of $D(p_{\varepsilon,\sigma,\tau})$, we do not pursue this issue any further. □

A.4. Versality conditions

It remains to check the versality condition (12) for the strata in the Whitney stratification of $D(p_{\varepsilon,\sigma,\tau})$. We first show that $p_{\varepsilon,\sigma,\tau}$ satisfies the versality conditions corresponding to points of

type A_4 at $(A_4)_1^{\pm}$ and $(A_4)_2^{\pm}$. Instead of checking (12) for these strata, we use an observation from [5] stating that $p_{\varepsilon,\sigma,\tau}$ is closely related to $s_{\varepsilon,\kappa,\lambda,\rho,\tau_1} : \mathbb{R}_+ \to \mathbb{R}$ given by

$$s_{\varepsilon,\kappa,\lambda,\rho,\tau_1}(u) = u^4 - \varepsilon u^{q-2} + 2\tau_1 u^3 + \rho u^2 + \lambda u + \kappa,$$

where $\rho, \kappa, \lambda, \tau_1 \in \mathbb{R}$. In fact, the set $D(p_{\varepsilon,\sigma,\tau})$ is the pull back of $D(s_{\varepsilon,\kappa,\lambda,\rho,\tau_1})$ under the singular map $\psi : \mathbb{R}^4 \to \mathbb{R}^4$ given by

$$\psi(\tau_1, \tau_2, \sigma_1, \sigma_2) \mapsto (\kappa, \lambda, \rho, \tau_1) = (\sigma_1^2 + \sigma_2^2, 2(\tau_1\sigma_1 + \tau_2\sigma_2), \tau_1^2 + \tau_2^2 + 2\sigma_1, \tau_1).$$

A short computation reveals that this map has at least rank 2 for small parameter values and the singular set of this map is given by

$$S(\psi) = \{(\tau_1, \tau_2, \sigma_1, \sigma_2) \big| \tau_2^2\sigma_1 - \tau_1\tau_2\sigma_2 + \sigma_2^2 = 0\}.$$

We recall that a subset of this set has appeared before as $D(p_{0,\sigma,\tau})$. By [4, 5, 33] the family $s_{\varepsilon,0,0,0,\tau_1}$ is right-equivalent to u^4 and $s_{\varepsilon,\kappa,\lambda,\rho,\tau_1}$ is a versal unfolding of the central singularity u^4 for all τ_1 near $\tau_1 = 0$. Consequently, the set $D(s_{\varepsilon,\kappa,\lambda,\rho,\tau_1})$ is the product of a real line and a geometry of type A_4 [4, 5, 33]. The relation between $D(s_{\varepsilon,\kappa,\lambda,\rho,\tau_1})$ and $D(p_{\varepsilon,\sigma,\tau})$ near $(A_4)_1^{\pm}$ and $(A_4)_2^{\pm}$ is made apparent in the following theorem.

Theorem A.4. *The map ψ maps $(A_4)_1^{\pm}$ and $(A_4)_2^{\pm}$ to a set of points of type A_4 of $s_{\varepsilon,\kappa,\lambda,\rho,\tau_1}$.*

Moreover, if $\tau_1 < 0$, then the geometry of type A_4 can locally around $\psi((A_4)_1^{\pm})$ and $\psi((A_4)_2^{\pm})$ be pulled back diffeomorphically to $D(p_{\varepsilon,\sigma,\tau})$ for $\varepsilon \neq 0$. Consequently, also $D(p_{\varepsilon,\sigma,\tau})$ shows this geometry near $(A_4)_1^{\pm}$ and $(A_4)_2^{\pm}$.

This theorem is clarified by figure 14 showing the geometry of type A_4 of $D(s_{0,\kappa,\lambda,\rho,0})$ and figure 13 showing the pull back of this geometry in $D(p_{\varepsilon,\sigma,\tau})$ near $(A_4)_2^{\pm}$.

Proof. The first claim is that the pair of curves $(A_4)_1^{\pm}$ and $(A_4)_2^{\pm}$ are mapped by ψ to the points of type A_4 of $D(s_{\varepsilon,\kappa,\lambda,\rho,\tau_1})$. This easily follows from the fact that the components of ψ are the coefficients of $p_{\varepsilon,\sigma,\tau}$ and $s_{\varepsilon,\kappa,\lambda,\rho,\tau_1}$, so ψ is an identity as far as the coefficients are concerned. The degeneracy of a zero of $p_{\varepsilon,\sigma,\tau}$ and $s_{\varepsilon,\kappa,\lambda,\rho,\tau_1}$ depends only on the coefficients, so all 3-fold degenerate points of $p_{\varepsilon,\sigma,\tau}$ map to the 3-fold degenerate points of $s_{\varepsilon,\kappa,\lambda,\rho,\tau_1}$.

For $\varepsilon \neq 0$ and $\tau_1 < 0$ a small neighbourhood of $(A_4)_1^{\pm}$ does not intersect with the singular set $S(\psi)$, which implies that the geometry of type A_4 near $\psi((A_4)_1^{\pm})$ can be pulled back diffeomorphically by ψ^{-1} to $D(p_{\varepsilon,\sigma,\tau})$. Using the relation between $S(\psi)$ and $D(p_{0,\sigma,\tau})$, we can prove that for $\varepsilon \neq 0$ the sets $(A_4)_1^{\pm}$ and $S(\psi)$ do not intersect by showing that given τ, the value of the σ_1 component of $(A_4)_1^{\pm}$ is larger than the maximal σ_1 value of $D(p_{0,\sigma,\tau})$. Indeed, by appendix A.2 the σ_1 component of $D(p_{0,\sigma,\tau})$ is parametrized by $-u(\tau_1+u)$, so its maximum value is $\tau_1^2/4$. On the other hand, for $(A_4)_1^{\pm}$ we first require a higher order approximation of $(\Gamma_1^{\varepsilon,\pm})_{\sigma_1}$ than given in (27), for which (27), (33) and (34) are used. Substituting these in $(\Gamma^{\varepsilon,\pm})_{\sigma_1}$ as given in (21) yields

$$(\Gamma_1^{\varepsilon,\pm})_{\sigma_1} = \frac{1}{4}\tau_1^2 + \frac{(q-4)(q-3)}{6}\varepsilon^{q-6}\left(\frac{-\tau_1}{2}\right)^{q-4} + O(\varepsilon^{2(q-6)}),$$

which is bigger than $\tau_1^2/4$ for $q \geqslant 7$, $\varepsilon \neq 0$ and $\tau_1 < 0$.

The proof is more involved for $(A_4)_2^{\pm}$. First, we need to compute $(\Gamma_4^{\varepsilon,\pm})_{\sigma_1}$ and $(\Gamma_4^{\varepsilon,\pm})_{\sigma_2}$ to higher order than given in theorem A.3. Using (21), (31) and (34), we obtain

$$(\Gamma_4^{\varepsilon,\pm})_{\sigma_1} = u^2 - \varepsilon^{(q-6)/2}u^{(q-2)/2} + O(\varepsilon^{q-6}), \tag{37}$$

$$(\Gamma_4^{\varepsilon,\pm})_{\sigma_2} = \mp\left(\sqrt{2}\varepsilon^{(q-6)/4}u^{(q+2)/4} + \frac{q-2}{2\sqrt{2}}\varepsilon^{3(q-6)/4}u^{3q/4-5/2}\right) + O(\varepsilon^{q-6}). \tag{38}$$

The stratum $(A_4)_2^{\pm}$ intersects with $D(p_{0,\sigma,\tau})$ if given τ there is a value of σ_1 and σ_2 on $D(p_{0,\sigma,\tau})$ that equal (37) and (38), respectively. Using the parametrization of $D(p_{0,\sigma,\tau})$ given

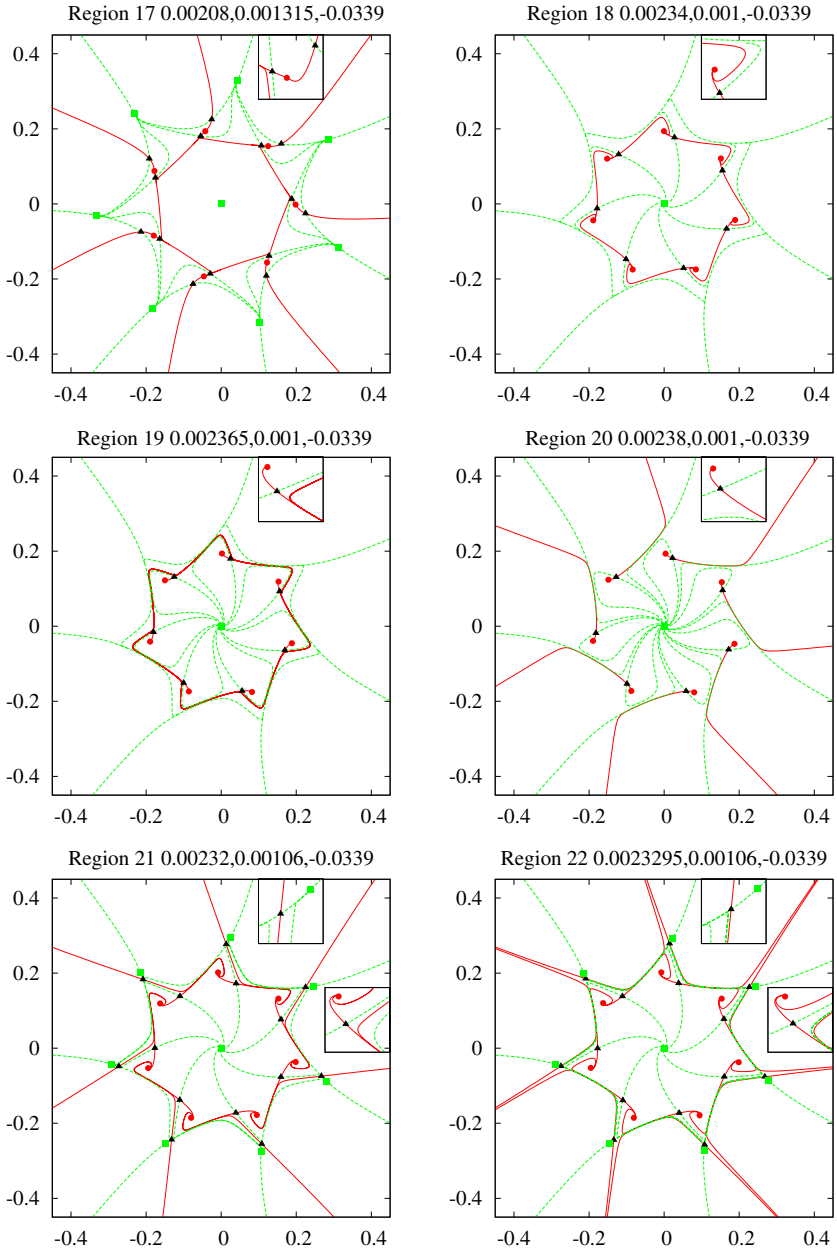

Figure 25. Phase portraits of the vector field $N_{\sigma,\tau}$ given in (19). The values of σ_1, σ_2 and τ_2, as well as the corresponding region in the parameter plane (see figure 21), are indicated on top of each plot. For the bifurcations that occur between neighbouring regions, we refer to figure 21.

in appendix A.2 this amounts to solving the following equations,

$$u_1^2 = u_2^2 - \varepsilon^{(q-6)/2} u_2^{(q-2)/2} + O(\varepsilon^{q-6}), \tag{39}$$

$$\sqrt{2}\varepsilon^{(q-6)/4} u_1^{(q+2)/4} = \sqrt{2}\varepsilon^{(q-6)/4} u_2^{(q+2)/4} - \frac{q-2}{2\sqrt{2}} \varepsilon^{3(q-6)/4} u_2^{3q/4-5/2} + O(\varepsilon^{q-6}). \tag{40}$$

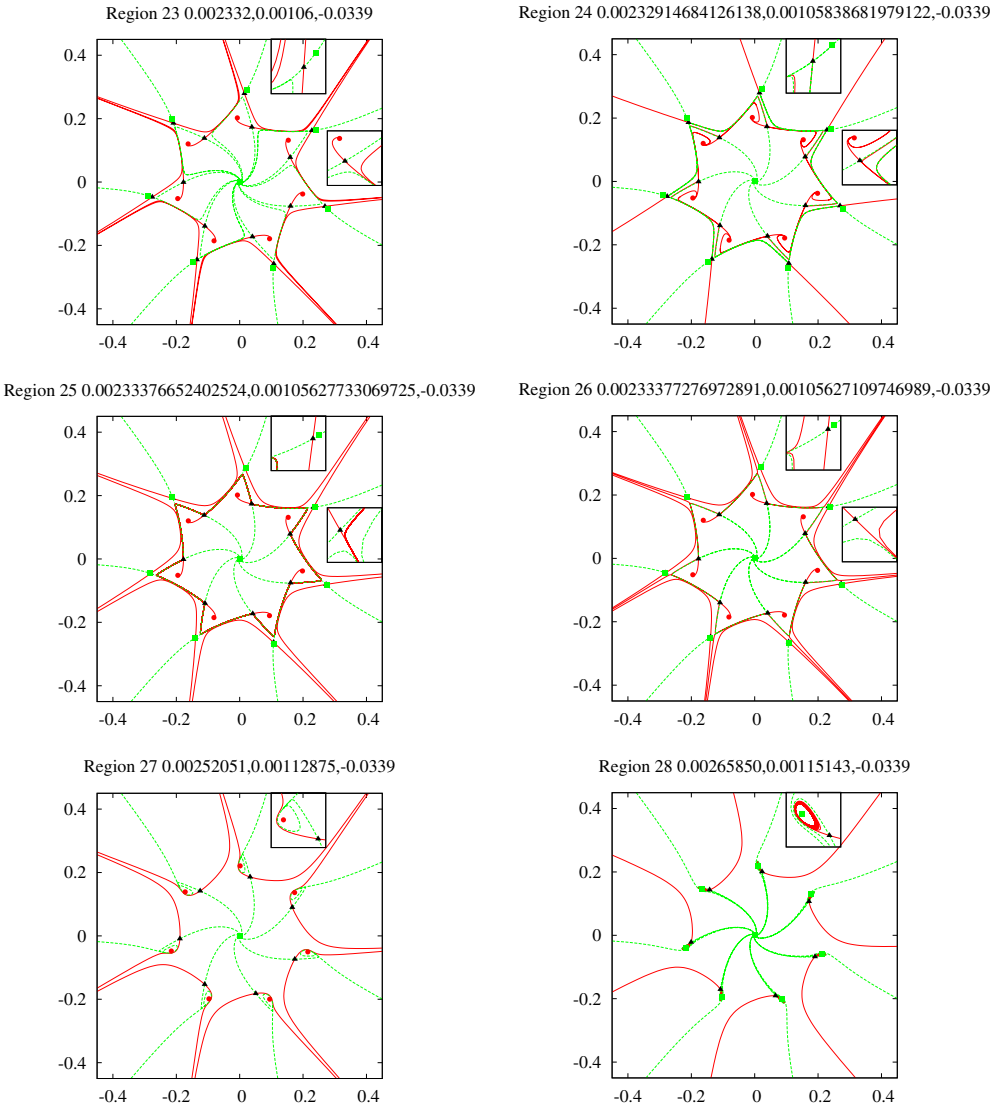

Figure 26. Continuation of figure 25. For the bifurcations that occur between neighbouring regions, we refer to figure 21.

Substituting u_1 as in (40) in the left hand side of (39) gives

$$\frac{q-2}{2}\varepsilon^{(q-6)/2}u_2^{(q-4)/2} = \varepsilon^{(q-6)/2}u_2^{(q-2)/2} + O(\varepsilon^{q-6})$$

Using (34), this equation reduces to

$$\frac{q-2}{2}\varepsilon^{(q-6)/2}\left(\frac{-\tau_1}{2}\right)^{(q-4)/2} = \varepsilon^{(q-6)/2}\left(\frac{-\tau_1}{2}\right)^{(q-2)/2} + O(\varepsilon^{q-6}),$$

which only holds for $\varepsilon = 0$ or $\tau_1 = 0$. The solution $\tau_1 = 2-q+O(\varepsilon^{(q-6)/2})$ can be discarded, since it is not close to zero. □

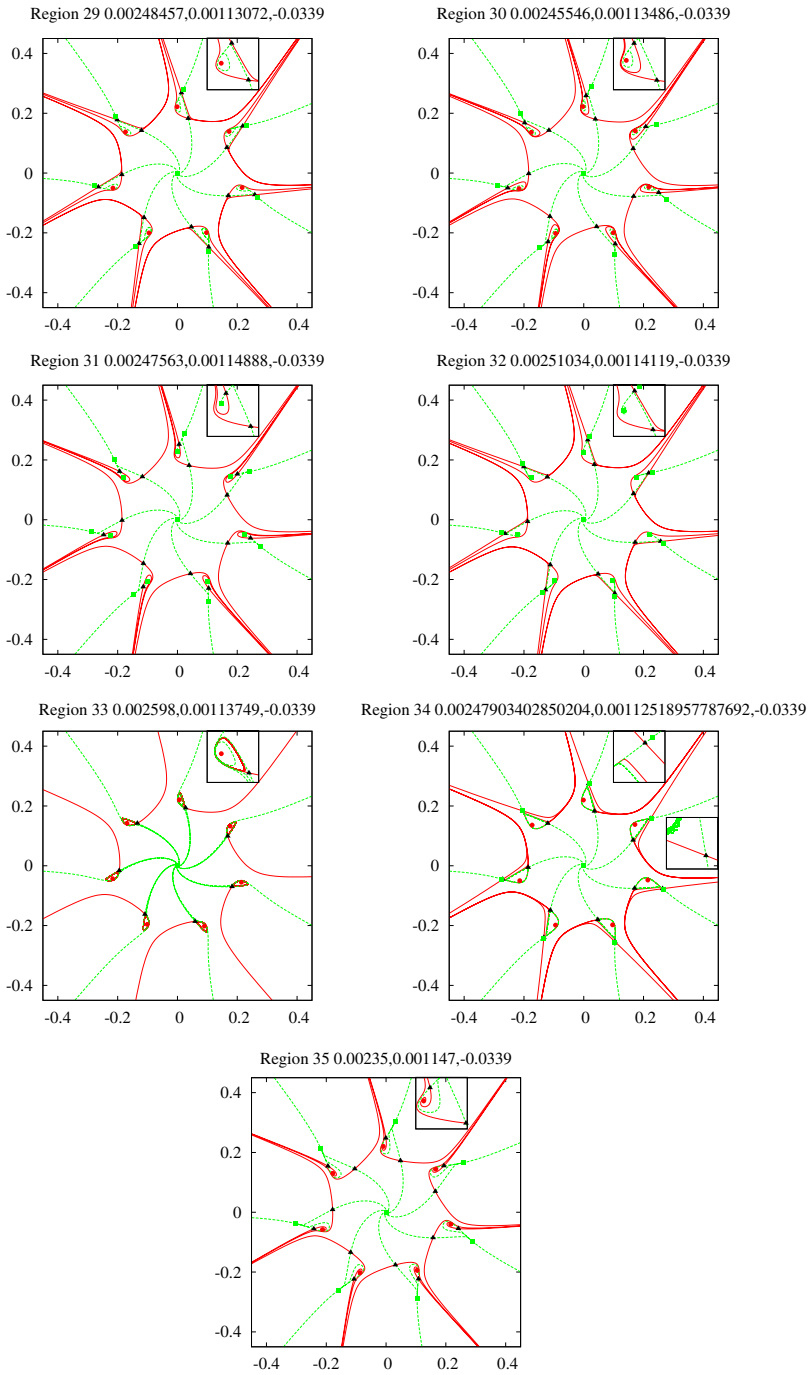

Figure 27. Continuation of figure 26. For the bifurcations that occur between neighbouring regions, we refer to figure 21.

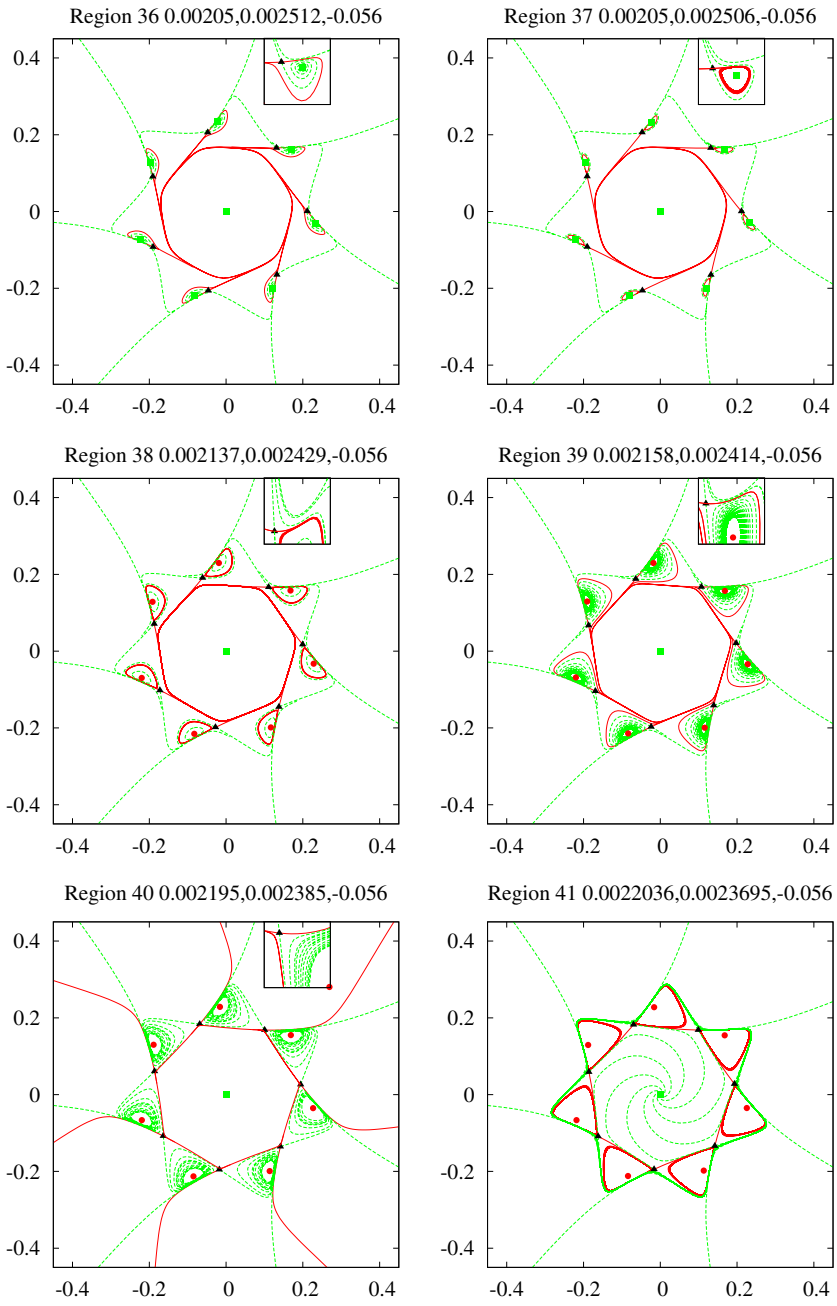

Figure 28. Continuation of figure 27. For the bifurcations that occur between neighbouring regions, we refer to figure 24.

The versality conditions of strata in $D(p_{\varepsilon,\sigma,\tau})$ of codimension less than 3 are checked by computing (12) explicitly. For points of type A_2 we obtain

$$\left.\frac{\partial(p_{\varepsilon,\sigma,\tau},(\partial p_{\varepsilon,\sigma,\tau}/\partial u))}{\partial(\sigma_1,\sigma_2,\tau_1,\tau_2)}\right|_{(\sigma,\tau)\in D(p_{\varepsilon,\sigma,\tau})} = \begin{pmatrix} \pm\frac{2\varepsilon^{\frac{q}{2}-3}\tau_2 u^{q/2}}{\sqrt{\tau_2{}^2+(\tau_1+2u)^2}} & 2(\tau_1+2u) \\ \mp\frac{2\varepsilon^{\frac{q}{2}-3}u^{q/2}(\tau_1+2u)}{\sqrt{\tau_2{}^2+(\tau_1+2u)^2}} & 2\tau_2 \\ \pm\frac{2\varepsilon^{\frac{q}{2}-3}\tau_2 u^{\frac{q}{2}+1}}{\sqrt{\tau_2{}^2+(\tau_1+2u)^2}} & 2u(\tau_1+2u)\pm\frac{2\tau_2 u^{q/2}\varepsilon^{\frac{q}{2}-3}}{\sqrt{\tau_2{}^2+(\tau_1+2u)^2}} \\ \mp\frac{2\varepsilon^{\frac{q}{2}-3}u^{\frac{q}{2}+1}(\tau_1+2u)}{\sqrt{\tau_2{}^2+(\tau_1+2u)^2}} & 2u\left(\tau_2\mp\frac{\varepsilon^{\frac{q}{2}-3}u^{\frac{q}{2}-1}(\tau_1+2u)}{\sqrt{\tau_2{}^2+(\tau_1+2u)^2}}\right) \end{pmatrix}.$$

Since the latter matrix has rank 2 for all points on $D(p_{\varepsilon,\sigma,\tau})$ the versality condition is also satisfied for all points of codimension less than 3.

To check the versality condition of $(R_qA_2)^{\pm}$ we cannot use $s_{\varepsilon,\kappa,\lambda,\rho,\tau_1}$, since $D(s_{\varepsilon,\kappa,\lambda,\rho,\tau_1})$ does not contain a stratum of type R_qA_2. Therefore, we verify directly whether closures of type R_q and type A_2 strata intersect transversally at $(R_qA_2)^{\pm}$. In the previous section we determined that R_q consists of parameter values for which $\sigma=0$ and $\tau\neq 0$, so the closures of strata intersect transversally if the following is non-zero

$$\det\left(\frac{\partial((\Gamma^{\varepsilon,\pm})_{\sigma_1},(\Gamma^{\varepsilon,\pm})_{\sigma_2})}{\partial(\tau_1,\tau_2)}\right)\Bigg|_{\tau\in(R_qA_2)^{\pm}} = \tau_1^2+O(\varepsilon^{q-6}).$$

The latter equation is non-zero, because $\tau_1\neq 0$ on $(R_qA_2)^{\pm}$.

A.5. Diffeomorphic two- and three-dimensional tomograms

In this section we determine all open regions of τ-values for which two-dimensional tomograms with τ fixed of $D(p_{\varepsilon,\sigma,\tau})$ for $\varepsilon\neq 0$ are diffeomorphic, see figure 15. By [4] we have that the boundary of such regions consists of the values for which a two-dimensional tomogram of parameter space with τ fixed is not transversal to a stratum of $D(p_{\varepsilon,\sigma,\tau})$ for $\varepsilon\neq 0$. We recall that two manifolds are transversal if they do not intersect or if their tangent spaces span the entire space at their intersection points. Consequently, strata of codimension 3 or 4 can only be transversal to a two-dimensional tomogram if they do not intersect. This means the boundaries of the open regions of interest are given by the projections of all codimension 3 and 4 strata on the τ-plane and by the projections of the curves $T^{\pm}$, since at these curves a two-dimensional tomogram is tangent to a codimension 2 stratum. Similar reasoning and using, e.g., figure 15 yields that three-dimensional tomograms with τ_1 fixed of $D(p_{\varepsilon,\sigma,\tau})$ are diffeomorphic for either positive values or negative values of τ_1.

B. Phase portraits for sections 3.2 and 3.3

Here we present phase portraits for section 3.2, in figures 25, 26 and 27 and also those for section 3.3, in figure 28. For explanation of the bifurcations between neighbouring regions we refer to sections 3.2 and 3.3. We note that if a region in parameter space occurs in more than one of the cases discussed in section 3, only one representative phase portrait is displayed.

References

[1] Arnol'd V I 1982 *Geometrical Methods in the Theory of Ordinary Differential Equations* (Berlin: Springer)
[2] Aronson D G, Chory M A, Hall R and McGehee R P 1983 Bifurcations from an invariant circle for two-parameter families of maps of the plane: a computer-assisted study *Commun. Math. Phys.* **83** 303–54

[3] Braaksma B L J and Broer H W 1987 On a quasi-periodic Hopf bifurcation *Ann. Inst. Henri Poincaré, Analyse Non Linéaire* **4** 114–68
[4] Bröcker T 1975 *Differential Germs and Catastrophes (London Mathematical Society Lecture Note Series)* (Cambridge: Cambridge University Press)
[5] Broer H W, Golubitsky M and Vegter G 2003 The geometry of resonance tongues: a singularity approach *Nonlinearity* **16** 1511–38
[6] Broer H W, Golubitsky M and Vegter G 2007 Geometry of resonance tongues *Proc. Workshop on Singularity Theory and its Applications (Marseille)* pp 327–56
[7] Broer H W, Holtman S J and Vegter G 2008 Recognition of the bifurcation type of resonance in mildly degenerate Hopf–Neĭmark–Sacker families *Nonlinearity* **21** 2463–82
[8] Broer H W, Simó C and Tatjer J C 1998 Towards global models near homoclinic tangencies of dissipative diffeomorphisms *Nonlinearity* **11** 667–770
[9] Broer H W, Simó C and Vitolo R 2008 The Hopf-saddle-node bifurcation for fixed points of 3D-diffeomorphisms: analysis of a resonance 'bubble' *Physica* D **237** 1773–99
[10] Broer H W and Simo C 2000 Resonance tongues in hill's equations: a geometric approach *J. Diff. Eqns.* **166** 290–327
[11] Broer H W and Vegter G 1992 Bifurcational aspects of parametric resonance *Dynamics Reported* (*New Series* vol 1) pp 1–51 (Berlin: Springer)
[12] Broer H W and Vegter G 2008 Generic Hopf–Neĭmarck–Sacker bifurcations in feed-forward systems *Nonlinearity* **21** 1547–78
[13] Chenciner A 1985 Bifurcations de points fixes elliptiques: II. orbites périodiques et ensembles de cantor invariants *Inventory Math.* **80** 81–106
[14] Chenciner A 1985 Bifurcations de points fixes elliptiques: I. Courbes invariantes *Publ. Math. IHES* **61** 67–127
[15] Chenciner A 1988 Bifurcations de points fixes elliptiques: III. Orbites périodiques de 'petites' périodes et elimination résonnantes des couples de courbes invariantes *Publ. Math. IHES* **66** 5–91
[16] Devaney R L 1989 *An Introduction to Chaotic Dynamical Systems* (Reading, MA: Addison-Wesley)
[17] Arnol'd V I (ed) 1993 *Dynamical systems VI: Singularity Theory I* (*Encyclopaedia of Mathematical Sciences* vol 6) (Berlin: Springer)
[18] Gibson C G, Wirthmüller K, du Plessis A A and Looijenga E J N 1976 *Topological Stability of Smooth Mappings* (*Lecture Notes in Mathematics* vol 552) (Berlin: Springer)
[19] Guckenheimer J and Holmes P 1983 *Nonlinear Oscillations, Dynamical Systems, and Bifurcations of Vector Fields* (Berlin: Springer)
[20] Il′yashenko Yu and Yakovenko S 1995 Finite cyclicity of elementary polycycles in generic families *Concerning the Hilbert 16th problem* (*American Mathematical Society Translations Series 2*, vol 165) (Providence, RI: American Mathematical Society) pp 21–95
[21] Jorba À and Zou M 2005 A software package for the numerical integration of ODEs by means of high-order Taylor methods *Exp. Math.* **14** 99–117
[22] Krauskopf B 1994 Bifurcation sequences at 1 : 4 resonance: an inventory *Nonlinearity* **7** 1073–91
[23] Kuznetsov Y A 1995 *Elements of Applied Bifurcation Theory* (*Applied Mathematical Sciences* vol 112) (Berlin: Springer)
[24] McGehee R P and Peckham B B 1995 Determining the global topology of resonance surfaces for periodically forced oscillator families ed W F Langford and W Nagata *Normal Forms and Homoclinic Chaos* (*Fields Institute Communications* vol 4) (Providence, RI: American Mathematical Soceity) pp 233–54
[25] McGehee R P and Peckham B B 1996 Arnold flames and resonance surface folds *Int. J. Bifurcations Chaos* **6** 315–36
[26] Mourtada A 1991 Cyclicité finie des polycycles hyperboliques de champs de vecteurs du plan. Algorithme de finitude *Ann. Inst. Fourier (Grenoble)* **41** 719–53
[27] Munkres J R 1999 *Topology* (Englewood Cliffs, NJ: Prentice Hall)
[28] Newhouse S E, Palis J and Takens F 1983 Bifurcation and stability of families of diffeomorphisms *Publ. Math. IHES* **57** 1–71
[29] Palis J and Takens F 1987 Hyperbolicity and the creation of homoclinic orbits *Ann. Math.* **125** 337–74
[30] Peckham B B, Frouzakis C E and Kevrekidis I G 1995 Bananas and banana splits: a parametric degeneracy in the Hopf bifurcation for maps *SIAM J. Math. Anal.* **26** 190–217
[31] Peckham B B and Kevrekidis I G 1991 Period doubling with higher-order degeneracies *SIAM J. Math. Anal.* **22** 1552–74
[32] Peckham B B and Kevrekidis I G 2002 Lighting Arnold flames: resonance in doubly forced periodic oscillators *Nonlinearity* **15** 405–28
[33] Poston T and Stewart I 1996 *Catastrophe Theory and its Applications* (New York: Dover)

[34] Reyn J W 1980 Generation of limit cycles from separatrix polygons in the phase plane *Geometrical Approaches to Differential Equations* (*Lecture Notes in Mathematics* vol 810) *Proc. 4th Scheveningen Conf., Scheveningen, The Netherlands 1979)* (Berlin: Springer) pp 264–89

[35] Roussarie R 1986 On the number of limit cycles which appear by perturbation of separatrix loop of planar vector fields *Bol. Soc. Brasil. Math.* **17** 67–101

[36] Simó C 1990 On the analytical and numerical approximation of invariant manifolds ed D Benest and C Froeschlé Méthodes Modernes de la Mecánique Céleste (Course given at Goutelas, France, 1989) (Paris: Editions Frontières) pp 285–329

[37] Takens F 1974 Forced oscillations and bifurcations *Applications of Global Analysis I* (Communications of the Mathematical Institute of the University of Utrecht) vol 3, pp 1–59 Reprinted in *Global Analysis of Dynamical Systems* Festschrift Dedicated to Floris Takens for his 60th Birthday (Leiden, 2001), ed H W Broer *et al* (Bristol: Institute of Physics) pp 1–61

[38] Thom R 1975 *Structural Stability and Morphogenesis* (New York: Addison Wesley)

[39] Vanderbauwhede A 1992 Branching of periodic solutions in time-reversible systems *Geometry and Analysis in Non-linear Dynamics* (*Pitman Research Notes in Mathematics* vol 222) (London: Pitman) pp 97–113

[40] van Strien S J 1979 Center manifolds are not smooth *Math. Z.* **166** 143–5

[41] Wolfram Research Inc. 2008 *Mathematica* version 7.0 (Champaign, IL: Wolfram Research Inc.)